Does Disabling Cloud Radiative Feedbacks Change Spatial Patterns of Surface Greenhouse Warming and Cooling?

Jason Chalmers,[a,b] Jennifer E. Kay,[a,c] Eleanor A. Middlemas,[a,c]
Elizabeth A. Maroon,[d] and Pedro DiNezio[c]

[a] Cooperative Institute for Research in Environmental Sciences, University of Colorado Boulder, Boulder, Colorado
[b] Department of Chemical Engineering, University of California, Santa Barbara, Santa Barbara, California
[c] Department of Atmospheric and Oceanic Sciences, University of Colorado Boulder, Boulder, Colorado
[d] Department of Atmospheric and Oceanic Sciences, University of Wisconsin–Madison, Madison, Wisconsin

ABSTRACT: The processes controlling idealized warming and cooling patterns are examined in 150-yr-long fully coupled Community Earth System Model, version 1 (CESM1), experiments under abrupt CO_2 forcing. By simulation end, $2 \times CO_2$ global warming was 20% larger than $0.5 \times CO_2$ global cooling. Not only was the absolute global effective radiative forcing ~10% larger for $2 \times CO_2$ than for $0.5 \times CO_2$, global feedbacks were also less negative for $2 \times CO_2$ than for $0.5 \times CO_2$. Specifically, more positive shortwave cloud feedbacks led to more $2 \times CO_2$ global warming than $0.5 \times CO_2$ global cooling. Over high-latitude oceans, differences between $2 \times CO_2$ warming and $0.5 \times CO_2$ cooling were amplified by familiar linked positive surface albedo and lapse rate feedbacks associated with sea ice change. At low latitudes, $2 \times CO_2$ warming exceeded $0.5 \times CO_2$ cooling almost everywhere. Tropical Pacific cloud feedbacks amplified the following: 1) more fast warming than fast cooling in the west, and 2) slow pattern differences between $2 \times CO_2$ warming and $0.5 \times CO_2$ cooling in the east. Motivated to quantify cloud influence, a companion suite of experiments was run without cloud radiative feedbacks. Disabling cloud radiative feedbacks reduced the effective radiative forcing and surface temperature responses for both $2 \times CO_2$ and $0.5 \times CO_2$. Notably, 20% more global warming than global cooling occurred regardless of whether cloud feedbacks were enabled or disabled. This surprising consistency resulted from the cloud influence on non-cloud feedbacks and circulation. With the exception of the tropical Pacific, disabling cloud feedbacks did little to change surface temperature response patterns including the large high-latitude responses driven by non-cloud feedbacks. The findings provide new insights into the regional processes controlling the response to greenhouse gas forcing, especially for clouds.

SIGNIFICANCE STATEMENT: We analyze the processing controlling idealized warming and cooling under abrupt CO_2 forcing using a modern and highly vetted fully coupled climate model. We were especially interested to compare simulations with and without cloud radiative feedbacks. Notably, 20% more global warming than global cooling occurred regardless of whether cloud feedbacks were enabled or disabled. This surprising consistency resulted from the cloud influence on forcing, non-cloud feedbacks, and circulation. With the exception of the tropical Pacific, disabling cloud feedbacks did little to change surface temperature response patterns including the large high-latitude responses driven by non-cloud feedbacks. The findings provide new insights into the regional processes controlling the response to greenhouse gas forcing, especially for clouds. When combined with estimates of cooling at the Last Glacial Maximum, the findings also help rule out large (4+ K) values of equilibrium climate sensitivity.

KEYWORDS: Climate sensitivity; Clouds; Greenhouse gases; Cloud radiative effects; Surface temperature

---

1. Introduction

Studies investigating the response of the climate system to an instantaneous carbon dioxide (CO_2) forcing date back to the earliest global climate modeling efforts (e.g., Manabe and Wetherald 1967; Manabe and Bryan 1985; Stouffer and Manabe 2003; Hansen et al. 2005). Since then, an immense literature has emerged using this idealized climate change framework. This framework provides direct quantification of the time scale and magnitude of the CO_2 influence on the climate response. Thus, these idealized experiments complement more realistic experiments that are transient (i.e., have temporally coincident forcing and response), more comparable to observations, and forced by much more than CO_2. Despite tremendous investment, key uncertainties and limitations remain. State dependent forcing and feedbacks affect climate sensitivity (e.g., Bloch-Johnson et al. 2020; Zhu and Poulsen 2020). Most fundamentally, it is unclear if climate sensitivity (the global mean temperature response) increases (e.g., Bloch-Johnson et al. 2020; Zhu and Poulsen 2020; Gregory et al. 2015; Jonko et al. 2013; Caballero and Huber 2013; Meraner et al. 2013), decreases (e.g., Colman and McAvaney 2009; Stouffer and Manabe 2003; Kutzbach et al. 2013) or varies non-monotonically (e.g., Mitevski et al. 2021) with subsequent carbon dioxide doublings. As for limitations, many existing studies have used models with relatively coarse

---

ⓐ Denotes content that is immediately available upon publication as open access.

Corresponding author: Jennifer. E. Kay, Jennifer.E.Kay@colorado.edu

horizontal resolution (2°+) and without realistic geography, dynamic ocean coupling, or cloud–aerosol interactions. Finally, many existing studies have relied exclusively on offline diagnostic analyses techniques to assess the influence of cloud processes, used suboptimal methods to quantify radiative forcing and feedbacks, and focused on global mean climate responses such as climate sensitivity while neglecting regional patterns and processes.

Given that clouds remain a central uncertainty for climate change, the influence of cloud radiative feedbacks on idealized CO_2 experiments merits further investigation. Under increased greenhouse gas scenarios, multiple lines of evidence suggest global cloud feedbacks are likely positive (Myers et al. 2021; Sherwood et al. 2020; Zelinka et al. 2017; Boucher et al. 2013). Almost all studies quantifying the impact of cloud feedbacks use offline diagnostic methods. Here, we focus on disabling cloud feedbacks or "cloud locking" to remove cloud radiative feedbacks from the climate response (e.g., Chen et al. 2021; Middlemas et al. 2020; Middlemas et al. 2019; Grise et al. 2019; Mauritsen et al. 2013). Actively removing cloud radiative feedbacks enables quantification of the full cloud feedback influence on the climate response. This cloud influence is found by differencing control and cloud locked simulations. As such, cloud influence diagnosed from cloud locking experiments offers new and complementary information to diagnostic cloud radiative feedbacks calculated offline. Importantly, cloud influence includes the cloud radiative feedback influence on radiative forcing, non-cloud feedbacks, and on circulation.

Cloud influence on the pattern of tropical surface ocean response is of particular interest. While tropical sea surface temperature (SST) changes are small in magnitude, they regulate tropical precipitation (e.g., Xie et al. 2010) and generate teleconnections well beyond the tropics (e.g., Alexander et al. 2002). The tropical SST pattern response to increasing CO_2 includes maximum warming along the equator, minimum warming in the southeast tropics, and a tendency for greater warming in the northern subtropics than the southern subtropics under increased greenhouse gases (Xie et al. 2010). This SST response is forced by the net surface flux and ocean circulation with damping by surface evaporation. Spatial pattern differences in the SST response are associated with wind pattern differences including westerly wind anomalies along the equator and trade wind changes in the subtropics. Though clouds are not always considered individually from surface heat fluxes, clouds strongly influence surface heat fluxes. For example, east–west asymmetries in the tropical Pacific net surface heat flux have been associated with cloud radiative effects (e.g., DiNezio et al. 2009; Meehl and Washington 1996). In addition to shaping SST patterns, clouds also respond strongly to the time evolution of the SST pattern. For example, recent work has used offline diagnostic techniques to suggest that delayed eastern tropical Pacific greenhouse warming is enhanced by positive cloud feedbacks (e.g., Dong et al. 2020; Andrews et al. 2015).

While a rich body of literature exists to study the influence of clouds on greenhouse warming, less has been done for greenhouse cooling. In addition to being of theoretical interest, understanding the processes that explain the differences between idealized greenhouse warming and cooling is a good first step toward understanding more complex warming and cooling climate phenomena. For example, idealized cooling is relevant for aerosol forcing, which can oppose the signal from increased greenhouse gases (e.g., Deng et al. 2020). That said, it is challenging to compare greenhouse cooling and aerosol cooling because of their differing spatiotemporal forcing patterns and their differing interactions with feedbacks, especially for clouds. Idealized cooling is also relevant to geoengineering, especially if technologies are developed that lead to rapid cooling. Finally, understanding idealized greenhouse cooling processes is also relevant for paleoclimate. While studies have highlighted the importance of cloud feedbacks for paleoclimate (e.g., Yoshimori et al. 2009; Zhu et al. 2019; Zhu et al. 2021), much remains unknown. Understanding cloud influence is especially important for the Last Glacial Maximum (LGM) which has recently been argued to provide a strong constraint on the upper bound on climate sensitivity (e.g., Tierney et al. 2020; Sherwood et al. 2020). Previous work found temperature-dependent cloud feedbacks operated differently during the LGM than for global warming (Yoshimori et al. 2009). At the LGM though, a lot changed in addition to greenhouse gases including orbital forcing, topography, sea level, surface albedo, vegetation, and aerosols. Thus, understanding the magnitude and mechanisms behind differences in idealized greenhouse cooling and warming is a first and fundamental step toward assessing whether estimates of climate sensitivity inferred from LGM cooling are relevant for future warming.

In this study, we analyze the climate response to idealized greenhouse warming and cooling in a widely used fully coupled Earth system model. We focus on $2 \times CO_2$ global warming and $0.5 \times CO_2$ global cooling as these are the climate states that are most relevant since the LGM and looking forward into the twenty-first century. We address two primary research questions:

1) To what extent are $2 \times CO_2$ global warning and $0.5 \times CO_2$ global cooling extent equal but opposite in their forcing and feedbacks?
2) Does disability cloud radiative feedbacks influence the climate response to $2 \times CO_2$ and $0.5 \times CO_2$ including especially the spatial patterns of surface temperature response?

While the first research question has been long explored in the literature, the second research question is new and unanswered. By disabling cloud radiative feedbacks–the most uncertain feedbacks in the climate system—we can complete an assessment of the climate system response to global warming and global cooling without them. Overall, we find cloud feedbacks amplify surface temperature responses, but the pattern of surface warming and cooling are remarkably similar with and without cloud radiative feedbacks at most locations on the globe. For example, high-latitude ocean response patterns and time evolution are controlled by sea ice and ocean circulation change but amplified by cloud feedbacks. One notable exception is that cloud feedbacks strongly shape the time evolution and amplitude of the tropical Pacific response.

TABLE 1. Description of model runs. All runs use the Community Earth System Model, version 1 with the Community Atmosphere Model, version 5 (CESM1-CAM5) at 1° horizontal resolution.

Name	Description	Years used	Reference
CNT	Fully coupled 1850 control	402–552	Kay et al. (2015)
CNT_2×CO$_2$	Abrupt 2 × CO$_2$ fully coupled 1850 control, used for ERF_reg 1	1–150	Frey and Kay (2018)
CNT_0.5×CO$_2$	Abrupt 0.5 × CO$_2$ fully coupled 1850 control, used for ERF_reg 1	1–150	This work
fSST	Fixed SST/sea ice 1850 control, SST/sea ice climatology from CNT years 402–1510	1–30	Kay et al. (2015)
fSST_2×CO$_2$	Abrupt 2 × CO$_2$ fixed SST/sea ice, initial condition fSST date = 006–01–01	1–30	This work
fSST_0.5×CO$_2$	Abrupt 0.5 × CO$_2$ fixed SST/seaice, initial condition fSST date = 006–01–01	1–30	This work
CNT_2×CO$_2$_1	As in CNT_2×CO$_2$ but initial condition from CNT date = 411–01–01, used for ERF_reg #2	1–20	This work
CNT_2×CO$_2$_2	As in CNT_2×CO$_2$ but initial condition from CNT date = 416–01–01, used for ERF_reg 3	1–20	This work
CNT_0.5×CO$_2$_1	As in CNT_0.5×CO$_2$ but initial condition from date = 411–01–01, used for ERF_reg 2	1–20	This work
CNT_0.5×CO$_2$_2	As in CNT_0.5×CO$_2$ but initial condition from date = 416–01–01, used for ERF_reg 3	1–20	This work
CL	Fully coupled 1850 control with cloud locking	1–150	Middlemas et al. (2020)
CL_2×CO$_2$	Abrupt 2 × CO$_2$ fully coupled 1850 control with cloud locking, used for ERF_reg 1	1–150	Middlemas et al. (2020)
CL_0.5×CO$_2$	Abrupt 0.5 × CO$_2$ fully coupled 1850 control with cloud locking, used for ERF_reg 1	1–150	This work
CL_fSST	As in fSST but with cloud locking	1–30	This work
CL_fSST_2×CO$_2$	As in fSST_2×CO$_2$ but with cloud locking	1–30	This work
CL_fSST_0.5×CO$_2$	As in fSST_0.5×CO$_2$, but with cloud locking	1–30	This work
CL_2×CO$_2$_1	As in CL_2×CO$_2$, but initial condition from CNT date = 411–01–01, used for ERF_reg 2	1–20	This work
CL_2×CO$_2$_2	As in CL_2×CO$_2$, but initial condition from CNT date = 416–01–01, used for ERF_reg 3	1–20	This work
CL_0.5×CO$_2$_1	As in CL_0.5×CO$_2$, but initial condition from CNT date = 411–01–01, used for ERF_reg 2	1–20	This work
CL_0.5×CO$_2$_2	As in CL_0.5×CO$_2$, but initial condition from CNT date = 411–01–01, used for ERF_reg 3	1–20	This work

2. Methods

In this study, we use a state-of-the-art fully coupled global Earth system model: Community Earth System Model, version 1 (CESM1) with the Community Atmosphere Model, version 5 (CESM1-CAM5) (Hurrell et al. 2013). CESM1-CAM5 is a widely used community model that performs well when evaluated using observations. For example, CESM1-CAM5 has the smallest biases of all models participating in phase 5 of the Coupled Model Intercomparison Projection (CMIP5) for global distributions of surface temperature and precipitation (Knutti et al. 2013). CESM1-CAM5 also improved upon long-standing climate model cloud biases (e.g., the global too few, too bright bias, Kay et al. 2012). CESM1-CAM5 simulations reasonably match observed warming since preindustrial (Meehl et al. 2013; Kay et al. 2015) and reconstructions of past extreme warm and cold climates (e.g., Eocene in Zhu et al. 2019, Last Glacial Maximum in DiNezio et al. 2018 and Zhu and Poulsen 2021).

We ran a comprehensive suite of idealized global warming and global cooling experiments using CESM1-CAM5 at 1° horizontal resolution with carbon nitrogen cycling on (Table 1). Following protocol outlined by Webb et al. (2017),

we instantaneously doubled and halved carbon dioxide concentrations from an 1850 preindustrial control simulation and ran for 150 years (CNT_2×CO$_2$ and CNT_0.5×CO$_2$ in Table 1). We next repeated the same two experiments but with the cloud radiative feedbacks disabled or "locked" (CL_0.5×CO$_2$ and CL_0.5×CO$_2$ in Table 1). Our cloud locking protocol follows Middlemas et al. (2020). Briefly, we disabled cloud radiative feedbacks by prescribing cloud radiative properties from an ENSO-neutral preindustrial year in the atmospheric model radiation calculations. As a result, cloud radiative feedbacks were disabled in our simulations while the rest of the climate system freely evolves. All responses were found through comparison to the overlapping 150 years of the corresponding 1850 control run.

Differentiating between feedbacks and radiative forcing including rapid adjustments is a formidable challenge with a long history. The climate response to an instantaneously forcing change follows the following well-known equation:

$$dTS = \frac{R - ERF}{\lambda}, \quad (1)$$

where dTS is the global mean surface temperature response (K), R is the TOA radiation imbalance (W m^{-2}), ERF is the

effective radiative forcing (W m^{-2}), and λ is the total feedback parameter (W m^{-2} K^{-1}). ERF includes both the instantaneous radiative forcing and rapid adjustments to it. From Eq. (1), it is clear that both differences in forcing and feedbacks can influence the surface temperature response. Thus, we next describe our methods to constrain both forcing and feedbacks, including cloud influence on both.

Though a log-linear relationship relating CO_2 concentration and radiative forcing is a convenient first-order approximation (e.g., Myhre et al. 1998), multiple lines of evidence show that $0.5 \times CO_2$ radiative forcing is not exactly equal-but-opposite to $2 \times CO_2$ radiative forcing. Recent line-by-line transfer model calculations reveal non-log-linear CO_2-forcing relationships for both the instantaneous (no rapid adjustments) (Byrne and Goldblatt 2014) and stratospheric-adjusted radiative forcing (Etminan et al. 2016). Particularly relevant here, Byrne and Goldblatt (2014) show that the absolute instantaneous radiative forcing for $0.5 \times CO_2$ (3.50 W m^{-2}) is 10% less than that for $2 \times CO_2$ (3.89 W m^{-2}). Yet the radiative transfer code in CESM1 (Iacono et al. 2008) is not a line-by-line radiative transfer model, but instead has been optimized for efficient global model calculations. Thus, we directly quantify radiative forcing in CESM1. We followed guidance from Forster et al. (2016) who argue that the effective radiative forcing (instantaneous forcing + rapid adjustments) is the most useful and practical method to estimate radiative forcing in global climate models and who offer specific advice on its calculation.

We calculated effective radiative forcing (ERF) using two methods. First, we used the fixed SST protocol (ERF_fSST). Originally introduced by Hansen et al. (2005), the ERF_fSST method was endorsed as the preferred method by Forster et al. (2016). In this method, 30-yr atmosphere-only experiments with fixed SST and sea ice from a fully coupled preindustrial control are run. ERF is then estimated as the global mean top-of-model radiative imbalance difference between the experiments with altered CO_2 concentrations (fSST_$0.5\times CO_2$, fSST_$2\times CO_2$) and the control (fSST). Because rapid adjustments by clouds increase ERF (e.g., Andrews et al. 2011), we ran a similar suite of ERF_fSST experiments with cloud radiative feedbacks disabled (CL_fSST, CL_fSST_$2\times CO_2$, CL_fSST_$0.5\times CO_2$ in Table 1). Second, we estimated ERF using linear regression and fully coupled simulations (Gregory et al. 2004), which we call ERF_reg following Forster et al. (2016). In this method, we regressed the first 20 years of global annual mean values of TOA energy imbalance and temperature change. In this regression, the Y intercept is an estimate of ERF, and the slope is an estimate of feedback parameter. Because individual ERF_reg estimates are noisy, we used regressions based on three different initial conditions (see simulations used for ERF_reg 1, ERF_reg 2, ERF_reg 3 in Table 1). We also ran a similar suite of ERF_reg experiments with cloud locking (Table 1).

We used two diagnostic techniques to calculate radiative feedbacks: radiative kernels (i.e., Soden et al. 2008) and simplified radiative transfer (i.e., Taylor et al. 2007). All feedbacks were normalized by global mean temperature change. Our kernel feedback calculations used radiative kernels specifically designed for CESM1-CAM5 (Pendergrass et al. 2018).

Cloud feedbacks were calculated as a residual, adjusted for non-cloud influence following Shell et al. (2008). We also analyzed shortwave radiative feedbacks calculated using the simplified radiative transfer model in the approximate partial radiative perturbation (APRP) technique (Taylor et al. 2007). Applying APRP in addition to radiative kernels was motivated by large changes to the mean state that can bias estimation of high-latitude shortwave cloud feedbacks using radiative kernels (e.g., Morrison et al. 2019). Specifically, differences between APRP and radiative kernel estimates of the shortwave cloud feedback arise from the treatment of surface albedo: APRP incorporates surface albedo changes when estimating feedbacks, while kernels do not. For this reason, we used APRP to calculate the shortwave cloud feedback including its contribution to the total cloud feedback. That said, comparisons between APRP and kernel-derived shortwave cloud feedbacks are shown. Because cloud feedbacks diagnosed with these techniques represent the influence of local clouds on surface temperature change, we call them "cloud feedbacks." In contrast, we use the term "cloud influence" when describing the result of differencing a control and cloud locked simulation. Cloud influence includes the cloud radiative feedback and also the coupling with of cloud feedbacks with circulation and the influence of cloud feedbacks on non-cloud feedbacks. Thus, unlike cloud feedbacks, cloud influence includes local surface temperature change driven by the coupling of remote cloud feedbacks with non-cloud feedbacks and circulation. Because the cloud locked simulation locks clouds at the preindustrial state, our estimate of cloud influence neglects the nonlinear interaction between radiative changes and the background environment (e.g., Colman and McAvaney 1997). Yet, a recent paper using cloud locking under $2 \times CO_2$ global warming (Chen et al. 2021) found that the impacts of this nonlinearity on cloud influence are small.

3. Results

a. Global surface temperature response, effective radiative forcing, and feedbacks

The global surface warming response to a carbon dioxide doubling ($2 \times CO_2$) was larger than the global surface cooling response to a carbon dioxide halving ($0.5 \times CO_2$) in fully coupled CESM1 simulations (Fig. 1a). This persistent surface temperature response difference occurred in all 150 years of the simulations providing evidence that it results from forcing and/or feedback differences, not internally driven climate variability. Based on averages over the last 50 years (years 100–150), the absolute magnitude of $2 \times CO_2$ global warming (2.73 K) exceeded the magnitude of $0.5 \times CO_2$ global cooling (2.28 K) by 0.47 K. More than 75% of these global surface temperature responses occurred in the first 50 years, accompanied by large decreases in the top-of-model energy imbalance. Unsurprisingly, the simulations remained ~1 W m^{-2} out of energy balance at year 150 (Fig. 1b). This residual energy imbalance reflects the multi-century time scales required for the ocean to reach equilibrium in a fully coupled model (e.g., Rugenstein et al. 2020; Stouffer 2004). This residual imbalance also implies additional surface temperature change
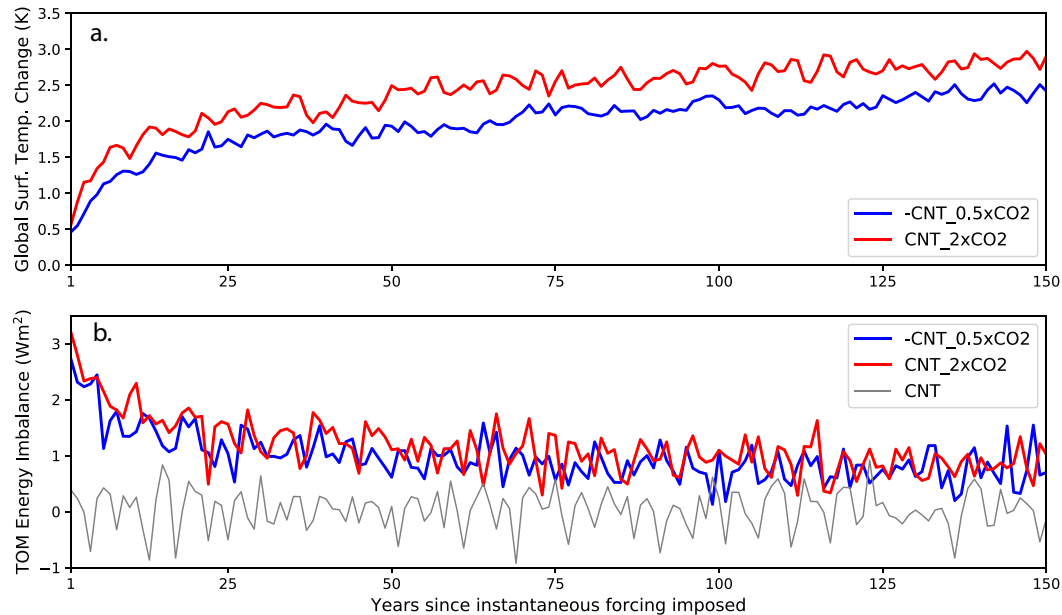
FIG. 1. Time series of global annual mean responses to instantaneous carbon dioxide forcing: (a) surface temperature change and (b) top-of-model (TOM) energy imbalance. All temperature changes are relative to CNT.

would occur if the simulations are extended. The similarity of the residual imbalance magnitude for $2 \times CO_2$ and $0.5 \times CO_2$ (Fig. 1b) and direct calculations of ocean heat uptake (not shown) both show that ocean heat uptake differences are not the first-order driver of $2 \times CO_2$ and $0.5 \times CO_2$ response differences.

Effective radiative forcing (ERF) differences help explain more $2 \times CO_2$ global warming than $0.5 \times CO_2$ global cooling. Indeed, two independent methods show that the globally averaged absolute ERF was larger for $2 \times CO_2$ than for $0.5 \times CO_2$ (Table 2). In other words, doubling carbon dioxide concentrations resulted in forcing that was close to, but not exactly equal-but-opposite forcing as halving carbon dioxide concentrations. The fixed SST method (ERF_fSST) shows

$2 \times CO_2$ ERF (3.82 ± 0.05 W m^{-2} was 10% larger than the absolute magnitude of the $0.5 \times CO_2$ ERF (3.44 ± 0.06 W m^{-2}). Similarly, the average of the regression method (ERF_reg) employed over the first 20 years with three different initial conditions shows the $2 \times CO_2$ ERF ($3.84 \pm$ standard error 0.69 W m^{-2}) was 15% larger than the absolute magnitude of the $0.5 \times CO_2$ ERF ($3.26 \pm$ standard error 0.58 W m^{-2}). Classic "Gregory" (Gregory et al. 2004) scatterplots of global top-of-model energy imbalance versus global surface temperature change following visually show a larger ERF (i.e., larger Y intercept) under $2 \times CO_2$ than under $0.5 \times CO_2$ (Fig. 2). That said, regression-based estimates of ERF were noisy with individual estimates of ERF deviating by over 10% and 95% confidence intervals that were an order of magnitude larger than those

TABLE 2. Global surface temperature change, effective radiative forcing, and global radiative feedbacks. Radiative feedbacks are estimated using radiative kernels over the last 50 year of the simulations. Uncertainties in the global mean surface temperature response and ERF are based on 95% confidence intervals following Forster et al. (2016). Maximum uncertainties in global feedbacks due to sampling are 0.03 W m^{-2} K^{-1} [see supporting information of Middlemas et al. (2020)].

| Description	CNT_2×CO$_2$	CNT_0.5×CO$_2$	CL_2×CO$_2$	CL_0.5×CO$_2$
Global mean surface temperature response (K)	2.75 ± 0.03	-2.28 ± 0.03	2.19 ± 0.03	-1.85 ± 0.02
ERF_fSST (W m^{-2})	3.82 ± 0.05	-3.44 ± 0.06	3.39 ± 0.03	-3.13 ± 0.04
ERF_reg (W m^{-2})	3.84 ± 0.69	-3.26 ± 0.58	3.51 ± 0.17	-3.24 ± 0.36
Total feedback parameter (W m^{-2} K^{-1})	-1.10	-1.19	-1.55	-1.66
Non-cloud feedbacks (W m^{-2} K^{-1})	-1.55	-1.43	-1.55	-1.66
Planck feedback (W m^{-2} K^{-1})	-3.19	-3.18	-3.18	-3.21
Surface albedo feedback (W m^{-2} K^{-1})	0.54	0.56	0.59	0.53
Lapse rate feedback (W m^{-2} K^{-1})	-0.42	-0.28	-0.28	-0.45
Water vapor feedback (W m^{-2} K^{-1})	1.52	1.47	1.32	1.47
Cloud feedback (W m^{-2} K^{-1})	0.45	0.24	0.00	0.00
Shortwave cloud feedback (W m^{-2} K^{-1})	0.34	0.11	—	—
Longwave cloud feedback (W m^{-2} K^{-1})	0.11	0.13	—	—
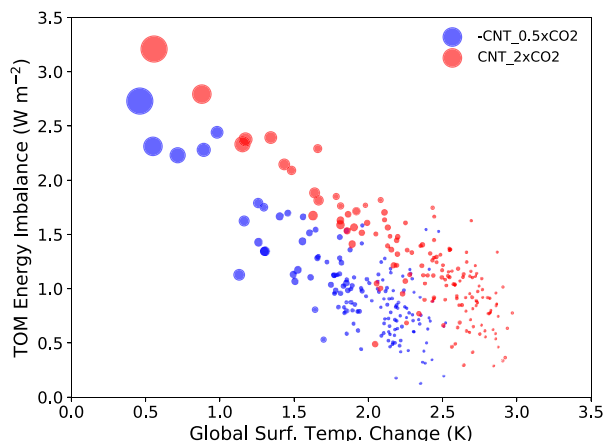
FIG. 2. "Gregory" (Gregory et al. 2004) scatterplot of top-of-model (TOM) energy imbalance ($W\,m^{-2}$) and global surface temperature change. Each point represents an annual average. The points decrease in size with time after the instantaneous carbon dioxide forcing was imposed. All temperature changes are compared to CNT.

estimated using ERF_fSST. Given these noisy results which are consistent with Forster et al. 2016, we place less emphasis on linear regression approaches to quantify ERF (Y intercept) and feedback (slope) differences.

In addition to forcing differences, radiative feedbacks also contribute to more $2 \times CO_2$ global warming than $0.5 \times CO_2$ global cooling. The global feedback parameter estimated by summing all kernel-based feedbacks was ~8% less negative under $2 \times CO_2$ global warming than under $0.5 \times CO_2$ global cooling (Table 2). This difference mostly arose from positive global cloud feedbacks that were almost twice as large under $2 \times CO_2$ global warming than under $0.5 \times CO_2$ global cooling.

Shortwave cloud feedback differences explain the $2 \times CO_2 - 0.5 \times CO_2$ cloud feedback differences though there was modest opposition by longwave cloud feedback differences. More positive global cloud feedbacks under global warming than under global cooling were opposed by a 50% more negative global lapse rate feedback under global warming than under global cooling. Global $2 \times CO_2 - 0.5 \times CO_2$ differences were small (within 4%) for the surface albedo, water vapor, and Planck feedbacks.

b. Regional surface temperature response and feedbacks

Typical regional temperature response patterns emerged by the end of the $2 \times CO_2$ global warming and $0.5 \times CO_2$ global cooling simulations (Figs. 3a,b). High-latitude surface temperatures responded more than low-latitude surface temperatures. This expected polar amplification of the surface temperature response coincides with the loss/gain of snow and sea ice cover (Manabe et al. 1990). In nonpolar regions, land surface temperatures responded more than SSTs. This expected land-ocean response contrast results from larger heat capacity, more efficient evaporation, and longer equilibrium time scales for the ocean when compared to the land (Sutton et al. 2007) and on moist static energy dynamics (Byrne and O'Gorman 2018). The North Atlantic Ocean surface temperature response opposed the global surface temperature response under both global warming and global cooling. This North Atlantic opposition results from the Atlantic meridional overturning circulation (AMOC) weakening under global warming and strengthening under global cooling, similar to the response seen in Stouffer and Manabe (2003) on this time scale.

While many expected responses were found, large regional pattern response differences between the $2 \times CO_2$ and $0.5 \times CO_2$ simulations were also evident (Figs. 3c,d). Land uniformly
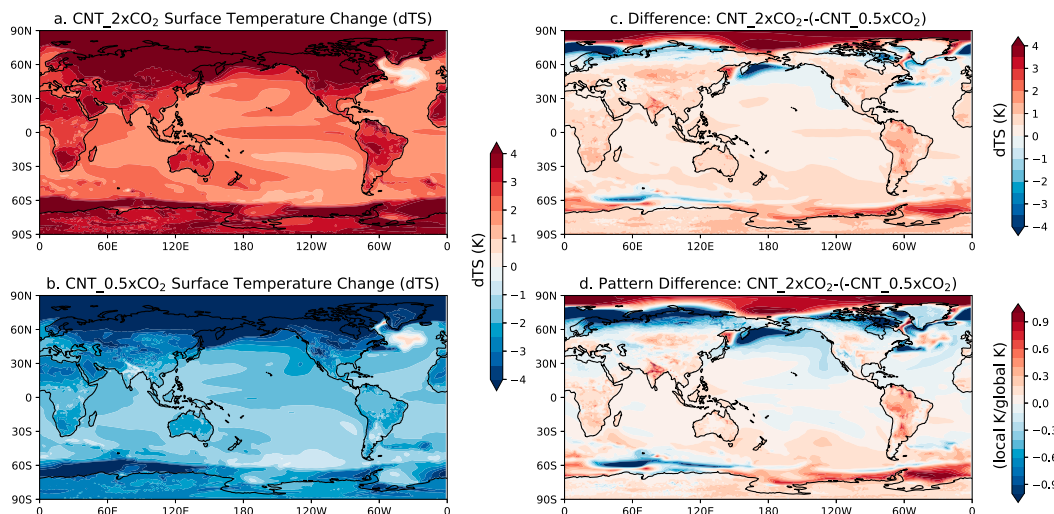

FIG. 3. Global maps of total surface temperature change from CNT for the last 50 years of simulations (years 100–150): (a) CNT_2×CO$_2$, (b) CNT_0.5×CO$_2$, (c) difference [CNT_2×CO$_2$ − (−CNT_0.5×CO$_2$)], and (d) pattern difference [CNT_2×CO$_2$ − (−CNT_0.5×CO$_2$)]. Pattern found by dividing local surface temperature change by the global mean surface temperature change.
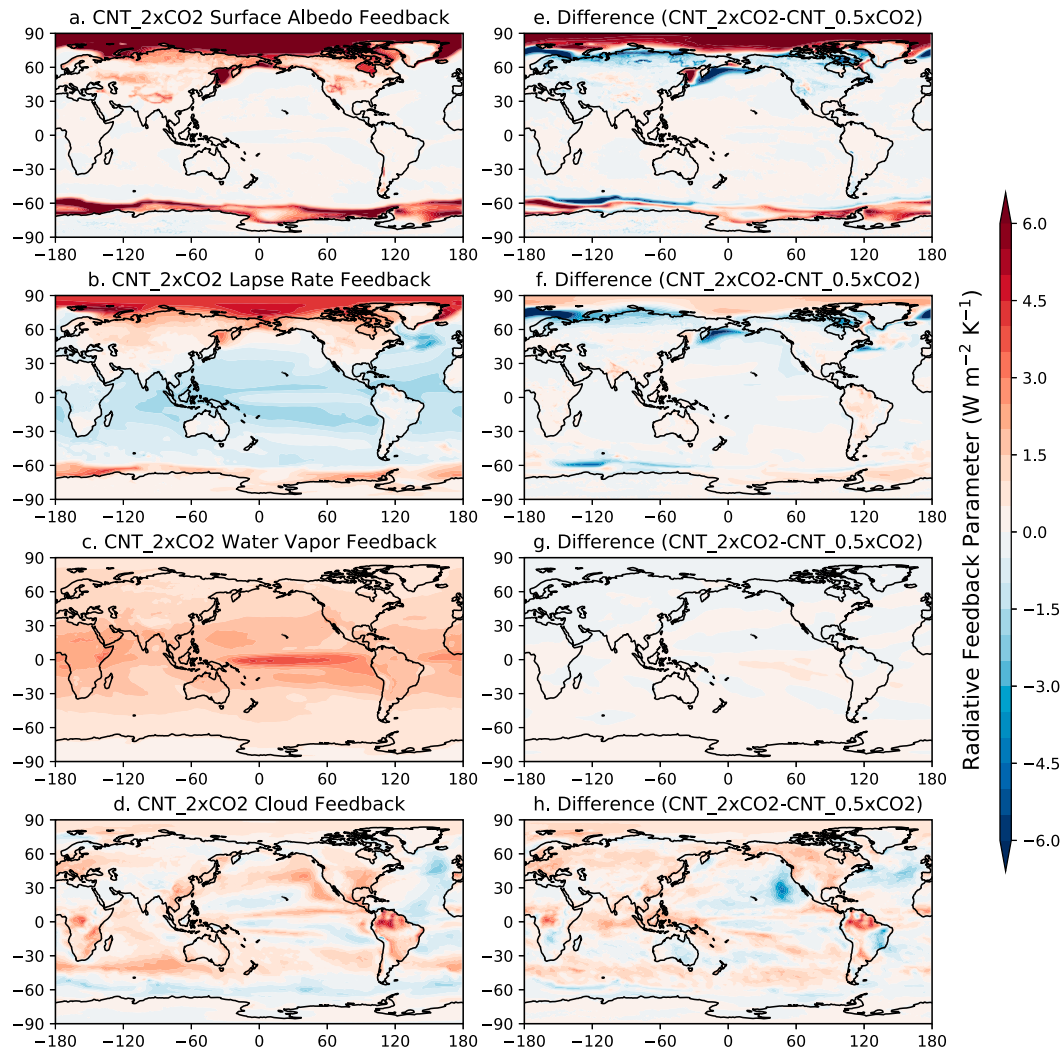
FIG. 4. Global maps of radiative feedbacks for the last 50 years of simulations (years 100–150): (a) CNT_$2\times CO_2$ surface albedo; (b) CNT_ $2\times CO_2$ lapse rate; (c) CNT_$2\times CO_2$ water vapor; (d) CNT_$2\times CO_2$ total cloud; and (e)–(h) as in (a)–(d), but for CNT_$2\times CO_2$ − CNT_$0.5\times CO_2$. Cloud feedbacks are the sum of shortwave component from APRP and longwave component from kernels.

experienced more $2 \times CO_2$ warming than $0.5 \times CO_2$ cooling with difference magnitudes ranging from 0.5 to 2 K. At high latitudes, the local temperature response differed by more than 3 K, spatially coinciding with sea ice response (not shown). Asymmetric warming occurred where sea ice retreated under $2 \times CO_2$ forcing, such as the high-latitude Arctic and around Antarctica. In contrast, asymmetric cooling occurred where sea ice advanced under $0.5 \times CO_2$ forcing, such as the Southern Ocean and over the North Pacific and Atlantic Oceans. The ice-free oceans generally experienced more $2 \times CO_2$ warming than $0.5 \times CO_2$ cooling by up to 1 K. One exception is the northeast Pacific off the coast of North America, where the surface ocean cooled more under $0.5 \times CO_2$ forcing than it warmed under $2 \times CO_2$ forcing. Enhanced cooling in this region was driven in part by advection of cold air generated by increased sea ice cover in the North Pacific (not shown).

We next assess where radiative feedbacks (Fig. 4) help explain surface temperature responses (Fig. 3). The Planck feedback by definition has a pattern that matches the surface temperature response pattern, and thus is not considered here. The $2 \times CO_2$ simulation provides a useful and familiar starting point. In response to $2 \times CO_2$, large positive surface albedo and lapse rate feedbacks amplified warming at high latitudes (Figs. 4a,b; Feldl et al. 2020; Manabe and Stouffer 1980), while negative lapse rate and positive water vapor feedbacks affected warming at low latitudes (Figs. 4b,c; Soden et al. 2008; Zhang et al. 1994). Water vapor feedbacks enhanced warming along the equatorial Pacific. A rich structure of mostly positive cloud feedbacks occurred at low latitudes (Figs. 4d) and showed some similarity to low-latitude warming patterns for example over the eastern tropical Pacific and South America (Fig. 3a).
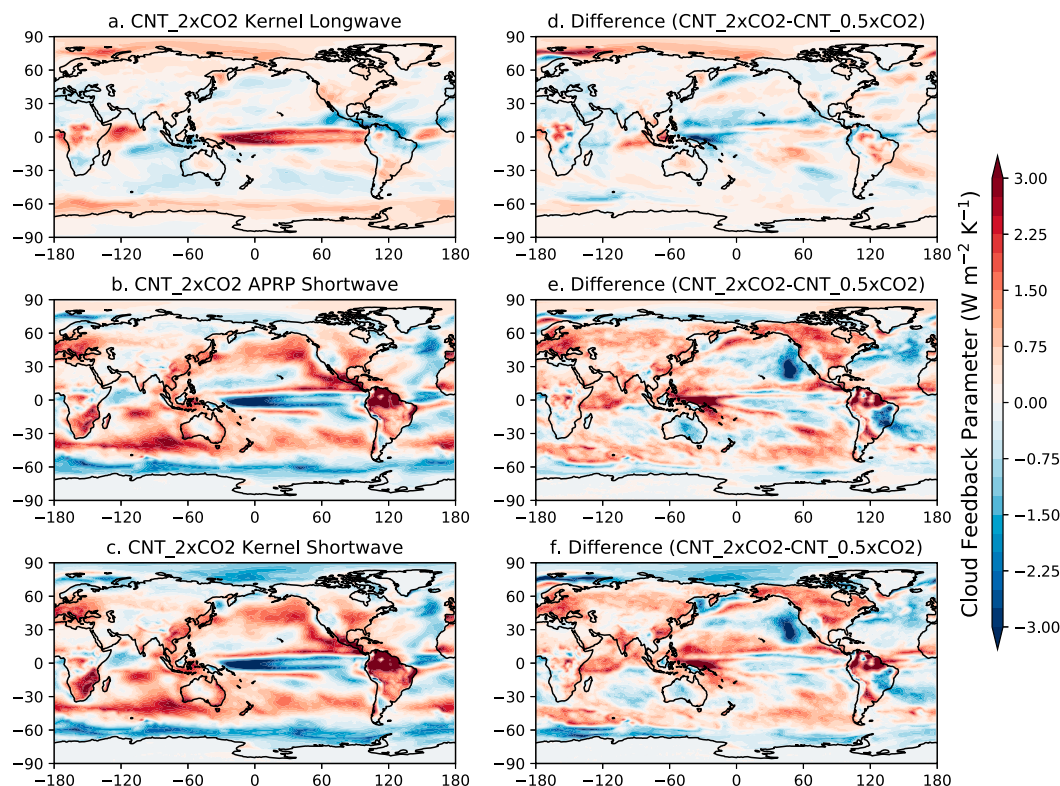
FIG. 5. Global maps of cloud feedbacks over the last 50 years of the simulations (years 100–150): (a) CNT_2×CO$_2$ longwave cloud feedback estimated using kernels, (b) CNT_2×CO$_2$ shortwave cloud feedback estimated using APRP, (c) CNT_2×CO$_2$ shortwave cloud feedback estimated using kernels; and (d)–(f) as in (a)–(c), but for the CNT_2×CO$_2$ − CNT_0.5×CO$_2$ difference.

With $2 \times CO_2$ as a reference, we next assess $2 \times CO_2$ − $0.5 \times CO_2$ feedback pattern differences and relate them to corresponding surface temperature pattern differences. At high latitudes, surface albedo and lapse rate feedbacks (Figs. 4e,f) amplified $2 \times CO_2$ − $0.5 \times CO_2$ surface temperature response differences (Figs. 3c,d). Specifically, large surface temperature responses resulting from positive surface albedo (6+ W m^{-2} K^{-1}) and lapse rate (3–5 W m^{-2} K^{-1}) feedbacks occurred where the sea ice edge retreated or advanced. For both the surface temperature response (Fig. 3) and radiative feedbacks (Fig. 4), differences between $2 \times CO_2$ and $0.5 \times CO_2$ had larger magnitudes at high latitudes than at low latitudes. Consistent with global averages (Table 2), cloud feedbacks (Fig. 4h) were more positive under $2 \times CO_2$ than under $0.5 \times CO_2$ in almost all locations. In addition, pattern matches between low-latitude cloud feedbacks and surface temperature responses emerged. For example, $2 \times CO_2$ − $0.5 \times CO_2$ cloud feedback differences (Fig. 4h) correspond with more $2 \times CO_2$ warming than $0.5 \times CO_2$ cooling over land especially in South America (Figs. 3c,d). Additionally, the northeast tropical Pacific cooled more than it warmed (Figs. 3c,d), consistent with $2 \times CO_2$ − $0.5 \times CO_2$ cloud feedback differences there (Fig. 4h).

Given the substantial $2 \times CO_2$ − $0.5 \times CO_2$ differences in cloud feedbacks, we assess shortwave and longwave cloud

feedback components individually (Fig. 5). Shortwave cloud feedback magnitudes exceeded longwave cloud feedback magnitudes almost everywhere. When present, the longwave cloud feedback opposed shortwave cloud feedback in the deep convective regions (e.g., along the equatorial tropical Pacific). For reasons discussed in the methods, we use APRP shortwave cloud feedbacks. Yet, kernel-based and APRP estimates of shortwave cloud feedbacks agree everywhere except high latitudes (Fig. 5).

While tropical responses have important influences on global responses, the magnitude of tropical SST change is relatively small, and benefits from tropical-specific color scaling. To that end, Fig. 6 emphasizes the rich pattern of tropical SST response and associated surface wind responses. For $2 \times CO_2$, this pattern includes well-known responses such as: 1) enhanced equatorial warming associated with anomalous westerly winds (Vecchi and Soden 2007; DiNezio et al. 2009; Xie et al. 2010), 2) more warming in the western than the eastern Indian Ocean associated with anomalous easterly winds (Ihara et al. 2009), and 3) a minimum in warming in the southern subtropics associated with hemispheric asymmetries in the trade wind response (Xie et al. 2010).

Differencing the tropical ocean responses to $2 \times CO_2$ and $0.5 \times CO_2$, we note more $2 \times CO_2$ warming than $0.5 \times CO_2$ cooling almost everywhere (Fig. 6c). More $2 \times CO_2$ warming
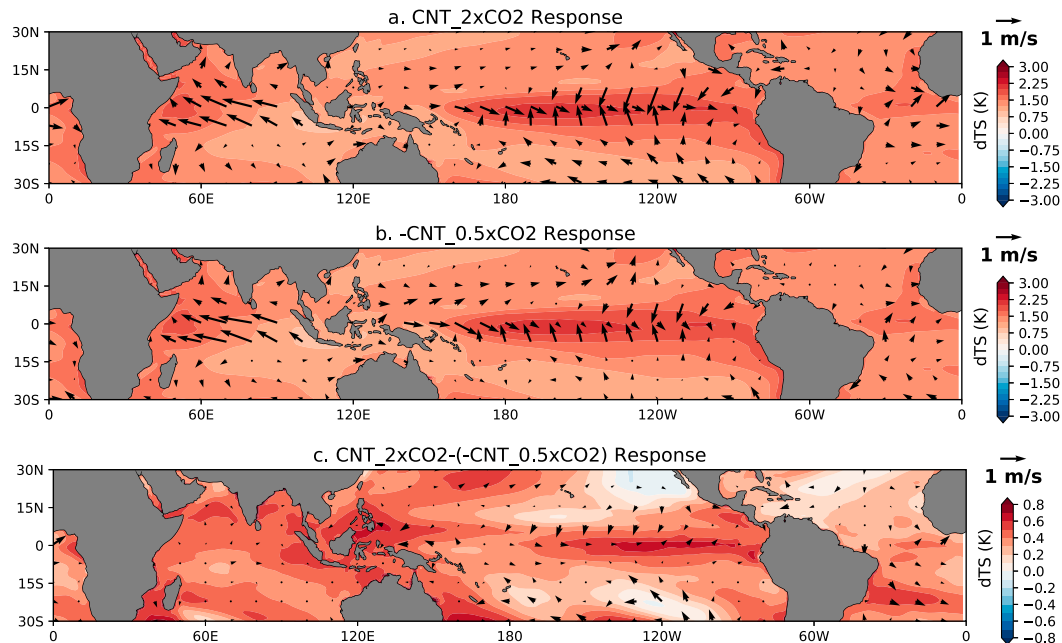
FIG. 6. Tropical ocean response over the last 50 years of the simulations (years 100–150): (a) CNT_2×CO$_2$ sea surface temperature (contours) and surface wind (arrows); (b) as in (a), but for CNT_0.5×CO$_2$; and (c) as in (a), but for the CNT_2×CO$_2$ − (−CNT_0.5×CO$_2$) difference. All responses are relative to CNT.

than 0.5 × CO$_2$ cooling was especially prominent in the convective western tropical Pacific, along the equator in the eastern Pacific, in the western and southeastern subtropical Pacific, and in the subtropical Indian and southern Atlantic Oceans. In contrast, more 0.5 × CO$_2$ cooling than 2 × CO$_2$ warming occurred in the subtropical northeast Pacific and subtropical North Atlantic. Surface wind response 2 × CO$_2$ − 0.5 × CO$_2$ differences were consistent with SST 2 × CO$_2$ − 0.5 × CO$_2$ response differences in some regions including along the equator. But, wind differences could not explain western tropical Pacific and the subtropical northeast Pacific 2 × CO$_2$ − 0.5 × CO$_2$ differences. Instead, normalizing by global mean responses emphasizes that these 2 × CO$_2$ − 0.5 × CO$_2$ pattern differences (Fig. 7a) match cloud feedback differences (Fig. 7a) and secondarily water vapor/lapse rate feedback differences (Fig. 7b). Unlike the tropical Pacific, a match between cloud feedbacks and surface temperature response patterns was less clear in the tropical Atlantic and Indian Ocean.

c. Time evolution of regional surface temperature patterns and feedbacks

We next contrast "slow" (years 50–150) and the "fast" (years 1–50) responses in our 2 × CO$_2$ and 0.5 × CO$_2$ simulations (Fig. 8). The slowest regions to respond were the North Atlantic and North Pacific, especially for 0.5 × CO$_2$. While Southern Ocean 2 × CO$_2$ warming was relatively slow, Southern Ocean 0.5 × CO$_2$ cooling was relatively fast. The largest magnitude slow surface temperature responses occurred at high northern latitudes for both 2 × CO$_2$ and 0.5 × CO$_2$ and at high southern latitudes for 2 × CO$_2$ (Figs. 8c,d).

High-latitude slow surface temperature responses (Fig. 8) and radiative feedbacks (Fig. 9) shared patterns in time and space. Over high northern latitude oceans, linked positive surface albedo and lapse rate feedbacks decreased in strength over time under 2 × CO$_2$ (Figs. 9a,b) but increased in strength over time under 0.5 × CO$_2$ (Figs. 9e,f). In the North Atlantic and North Pacific, the strengthening of these positive feedbacks with time enhanced delayed 0.5 × CO$_2$ cooling (Fig. 8b). Similarly, these positive feedbacks weakened with time in the Western Arctic Ocean matching relatively fast 2 × CO$_2$ warming there (Fig. 8a). Sea ice changes explained the high-latitude surface albedo and surface temperature response time evolution (Fig. 10). Notably, 2 × CO$_2$ Northern Hemisphere sea ice loss occurred almost entirely in the first 50 years with small and increasingly higher-latitude loss in subsequent years. While large 0.5 × CO$_2$ Northern Hemisphere sea ice gains occurred in the first 50 years, ice gain was also appreciable over the last 100 years of the simulation. Over mid–high southern latitude oceans, positive surface albedo and lapse rate feedbacks got stronger with time under 2 × CO$_2$ and weaker with time under 0.5 × CO$_2$ (Fig. 9). These changes were consistent with relatively fast sea ice expansion under 0.5 × CO$_2$ and slow sea ice retreat under 2 × CO$_2$ over the Southern Ocean (Fig. 10).

At low and midlatitudes, cloud feedbacks (Figs. 9d,h) changed the most through time and helped explain the time evolution of the surface temperature response. For example, positive cloud feedbacks over land decreased with time, consistent with relatively fast surface temperature responses there (Fig. 8). Over southern midlatitudes, 2 × CO$_2$ cloud feedbacks became more positive with time consistent with
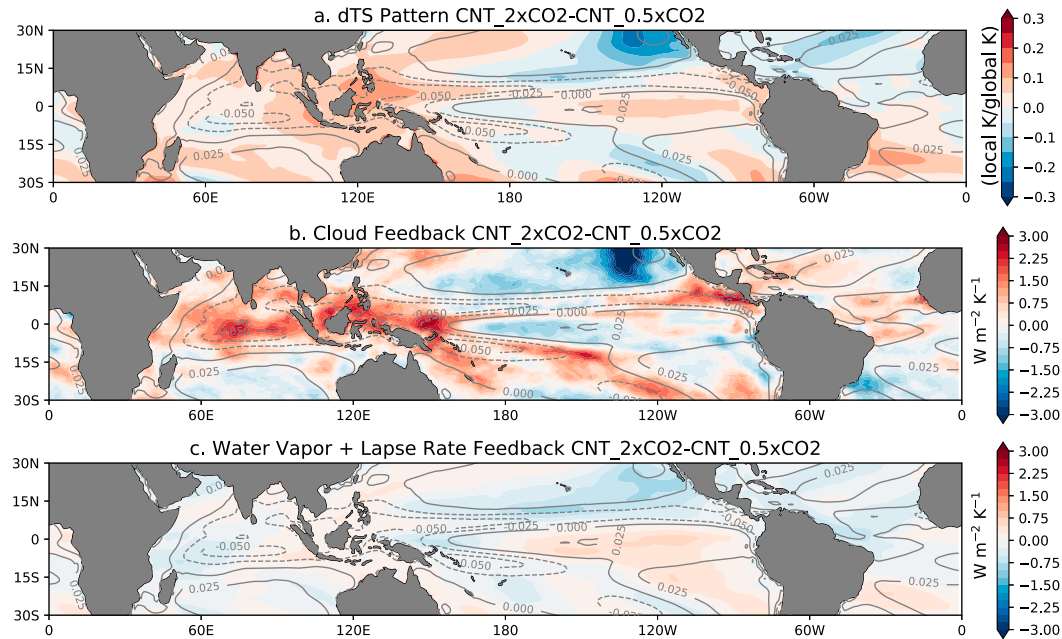
FIG. 7. Tropical oceans CNT_2×CO₂ − CNT_0.5×CO₂ difference from CNT for the last 50 years of the simulations (years 100–150): (a) sea surface temperature pattern, (b) cloud feedbacks, and (c) water vapor + lapse rate feedbacks. CNT 500-hPa subsidence (Pa s⁻¹) plotted in gray contours. Pattern found by dividing local surface temperature change by the global mean surface temperature change.

delayed 2 × CO₂ warming there. Under both 2 × CO₂ and 0.5 × CO₂, delayed eastern Pacific Ocean and northeastern Atlantic Ocean surface temperature responses were especially enhanced by positive cloud feedbacks.

The time evolution of tropical SST responses was driven by ocean dynamics and enhanced by cloud feedbacks (Fig. 11).

Sea surface temperatures in the eastern tropical Pacific were slow to respond to greenhouse forcing because they were controlled by upwelling of waters that have not yet come to equilibrium (e.g., DiNezio et al. 2009). This slower warming ultimately propagates to the central and western Pacific via the wind–SST–evaporation feedback. Under both 2 × CO₂
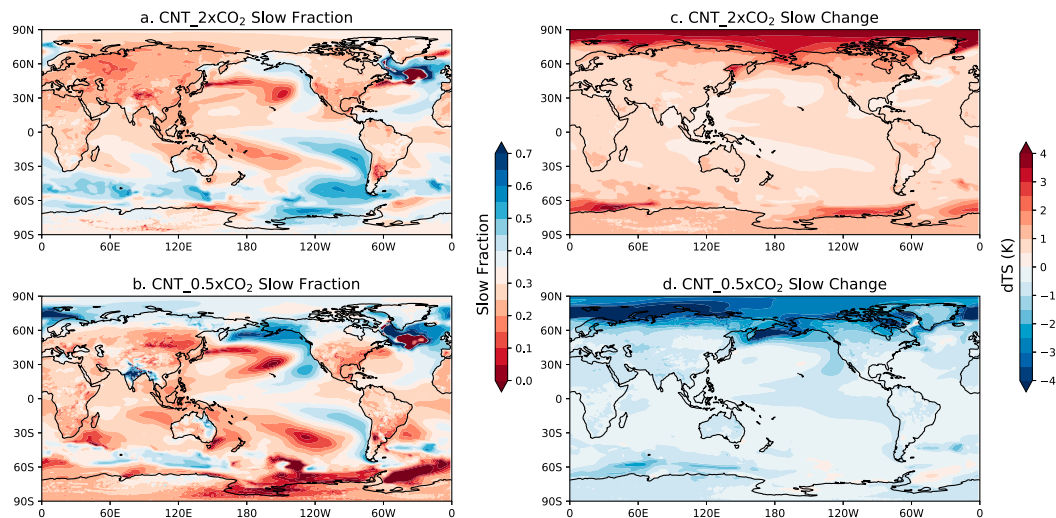
FIG. 8. Global maps of the surface temperature change (dTS): (a) CNT_2×CO₂ slow fraction, (b) CNT_0.5×CO₂ slow fraction, (c) CNT_2×CO₂ slow change, and (d) CNT_0.5×CO₂ slow change. The slow fraction is the fraction of the total change (years 100–150) that occurs after year 50. "Slow change" change is the total change (years 100–150) minus the "fast" change (years 1–50). In other words, slow change is the change that occurs after year 50.
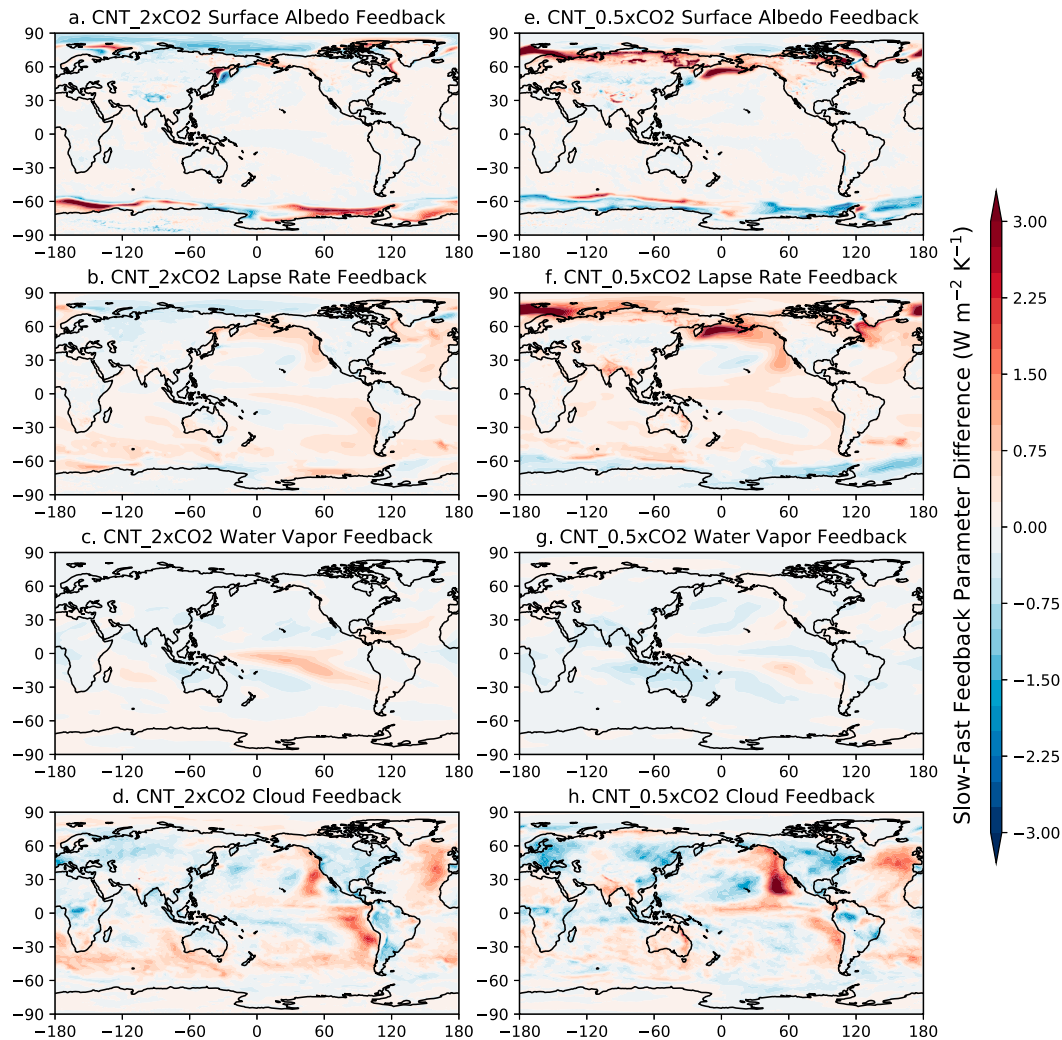
FIG. 9. As in Fig. 4, but showing the difference between slow (years 100–150) and fast (years 1–50) feedbacks for CNT_2×CO₂ and CNT_0.5×CO₂. Note: Color scale is half of that in Fig. 4.

and $0.5 \times CO_2$, this delayed eastern Pacific surface tempera-ture response (Figs. 11a,d) was enhanced by positive cloud feedbacks (Figs. 11b,e), with second-order contributions from positive lapse rate and water vapor feedbacks (Figs. 11c,f). The largest influence of cloud radiative feedbacks was on the slow $0.5 \times CO_2$ northeastern subtropical Pacific warming and the slow $2 \times CO_2$ southeastern subtropical Pacific cooling.

d. Understanding cloud influence by disabling cloud radiative feedbacks

"Cloud influence" (i.e., the difference between a control and a cloud locked simulation) increased both $2 \times CO_2$ global warming and $0.5 \times CO_2$ global cooling (Fig. 12). Specifically, enabling cloud radiative feedbacks increased the global sur-face temperature response measured using the last 50 years of the simulations (years 100–150) by 20%. A larger global sur-face temperature response with cloud radiative feedbacks enabled than with cloud radiative feedbacks disabled is

consistent with the positive global cloud feedbacks diagnosed using kernels/APRP (Table 2). Interestingly, both the residual top-of-model energy imbalance (Fig. 12b) and direct calcula-tions show that global ocean heat uptake is unaffected by dis-abling cloud feedbacks.

Fixed SST experiments show that enabling cloud feedbacks increased the absolute global mean ERF by 10% for both $2 \times CO_2$ and $0.5 \times CO_2$ (Table 2). Clouds rapidly adjusted to the CO_2 changes and those rapid cloud adjustments increased the strength of the CO_2 forcing in the control simulations as com-pared to the cloud locked simulations. Regression-based esti-mates also provided evidence for larger ERF with cloud feedbacks active than with cloud feedbacks disabled (Table 2). That said, regression-based estimates of ERF were noisy with individual estimates deviating by nearly 10%.

Surprisingly, enabling cloud feedbacks increased the global mean total feedback parameter by a similar amount for $2 \times CO_2$ ($+0.45 \text{ W m}^{-2} \text{ K}^{-1}$) and $0.5 \times CO_2$ ($+0.47 \text{ W m}^{-2} \text{ K}^{-1}$).
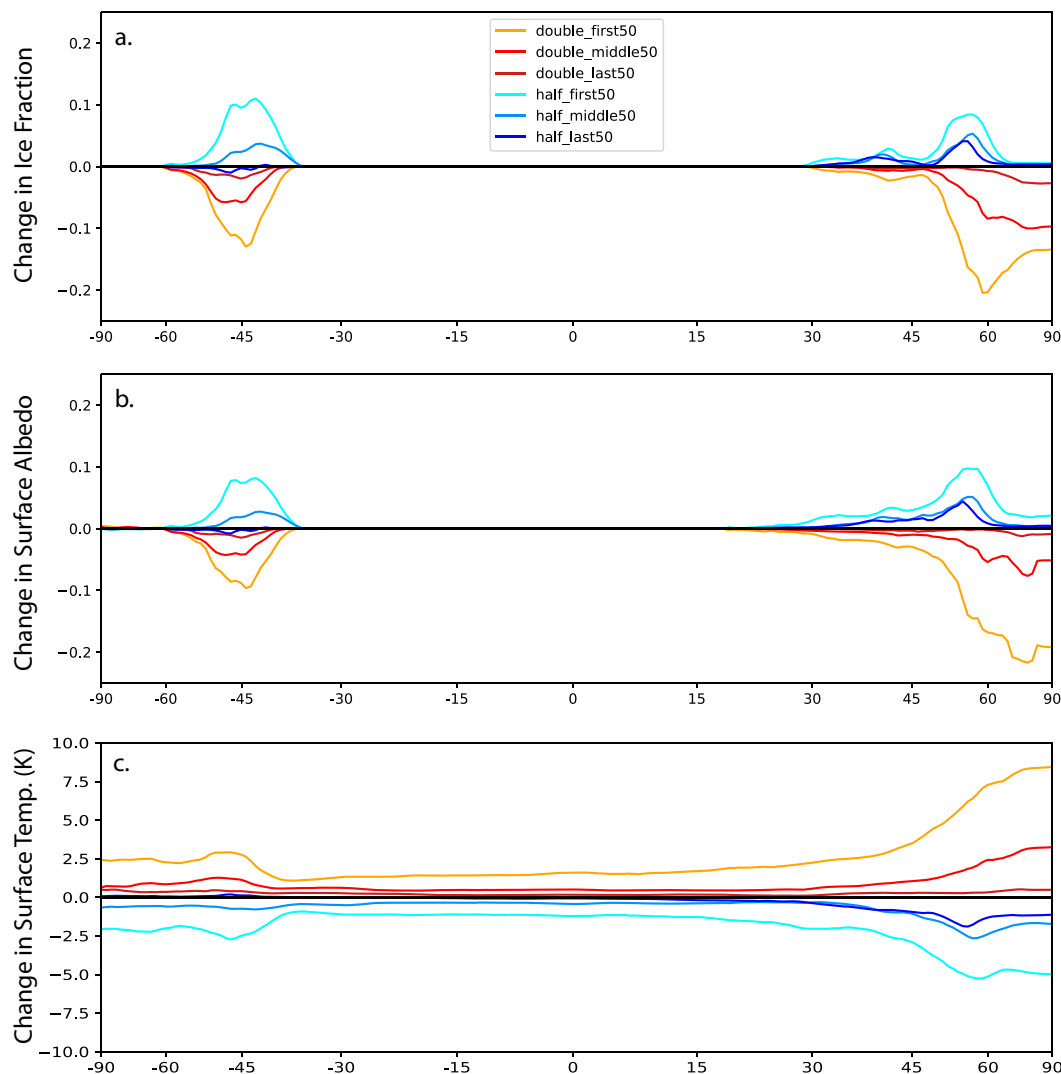
FIG. 10. Zonal annual mean time evolution: (a) change in sea ice fraction during the first 50 years (1–50), middle 50 years (51–100), and last 100 years (101–150). (b) As in (a), but for surface albedo change. (c) As in (a), but for surface temperature change.

Thus, cloud influence barely changed the total $2 \times CO_2 - 0.5 \times CO_2$ global feedback parameter difference (Table 2). Initially, this result seems surprising because the global mean cloud feedback was 0.21 W m^{-2} K^{-1} larger for $2 \times CO_2$ than for $0.5 \times CO_2$. But clouds can affect non-cloud feedbacks (Table 2, Fig. 13). Taken together, global cancellation between cloud influence on non-cloud feedbacks occurred under $2 \times CO_2$, but not under $0.5 \times CO_2$. As a result, cloud influence on non-cloud feedbacks reduced the $2 \times CO_2 - 0.5 \times CO_2$ global feedback parameter difference by 0.23 W m^{-2} K^{-1}, almost entirely compensating for the $2 \times CO_2 - 0.5 \times CO_2$ cloud feedback parameter difference of 0.21 W m^{-2} K^{-1}.

Globally for $2 \times CO_2$, cloud influence weakened the positive global surface albedo feedback by 0.05 W m^{-2} K^{-1}, strengthened the negative global lapse rate feedback by 0.14 W m^{-2} K^{-1}, and strengthened the positive water vapor feedback by

0.20 W m^{-2} K^{-1} (Table 2). Spatially for $2 \times CO_2$, there was compensation between cloud influence on high-latitude surface albedo/lapse rate feedbacks and tropical water vapor feedbacks (Fig. 13). But increases in the positive tropical water vapor feedback overpowered decreases in the high-latitude positive surface albedo and lapse rate feedbacks. In contrast to $2 \times CO_2$, cloud influence strengthened the $0.5 \times CO_2$ positive global surface albedo feedback by 0.03 W m^{-2} K^{-1}, weakened the negative $0.5 \times CO_2$ global lapse rate feedback by 0.17 W m^{-2} K^{-1}, and had no effect on the $0.5 \times CO_2$ water vapor feedback. Unlike for $2 \times CO_2$, cloud influence on tropical water vapor feedbacks was small for $0.5 \times CO_2$. Additionally, cloud influence was opposite in sign for $2 \times CO_2$ and $0.5 \times CO_2$ for high-latitude lapse rate and surface albedo feedbacks.

Enabling cloud feedbacks increased the surface temperature response to $2 \times CO_2$ and $0.5 \times CO_2$ at most locations on
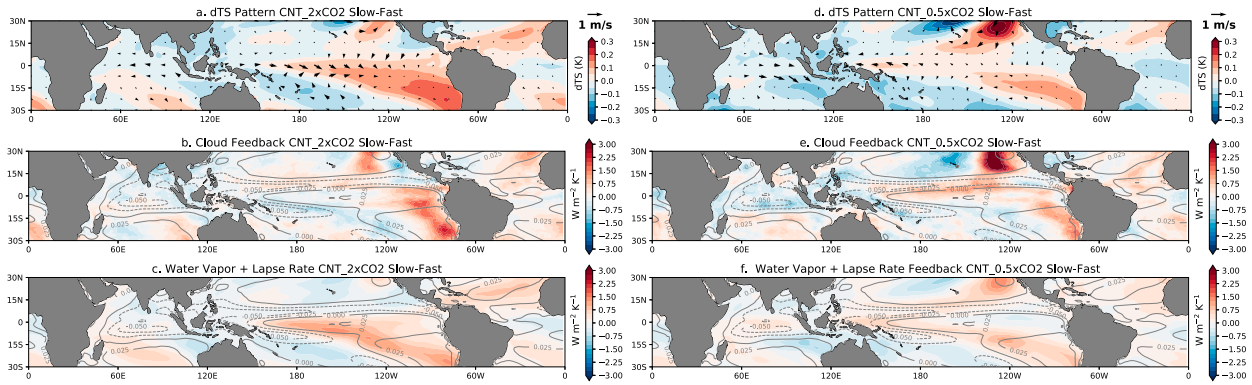
FIG. 11. Tropical ocean slow (years 100–150) minus fast (years 1–50). Response: (a) CNT_2×CO2 sea surface temperature pattern (colors; K) and surface wind (arrows; m s^{-1}); (b) CNT_2×CO2 cloud feedback (colors; W m^{-2} K^{-1}) and CNT 500-hPa subsidence (lines; Pa s^{-1}); (c) CNT_2×CO2 water vapor + lapse rate feedback; and (d)–(f) as in (a)–(c), but for CNT_0.5×CO2.

the globe (Fig. 14). Interestingly, enabling cloud feedbacks amplified surface temperature response patterns unassociated with cloud feedback patterns. As a result, global pattern correlations between simulations with cloud feedbacks enabled and disabled were high for 2 × CO$_2$ (0.99) and 0.5 × CO$_2$ (0.89). In addition, cloud influence patterns (Fig. 14) did not match total cloud feedback patterns (Figs. 4d,h) in most regions. The global pattern correlation between cloud influence and cloud feedback was small: 0.23 for 2 × CO$_2$ and −0.08 for 0.5 × CO$_2$.

Cloud influence increased the high northern latitude response despite small high-latitude cloud feedbacks. In other words, cloud influence on high northern latitude surface temperature did not result from local cloud feedbacks, but instead from low-latitude cloud feedbacks including their influence

on non-cloud feedbacks and circulation. The lapse rate and surface albedo feedbacks at high latitudes were important for explaining cloud influence on high-latitude surface temperature response pattern.

While not generally found, local correspondence between cloud influence (Figs. 14a,b) and cloud feedback (Figs. 4d,h) patterns did occur in some regions. For example, cloud influence affected the Southern Ocean response away from the sea ice edge, consistent with an equatorward transition from negative to positive cloud feedbacks there. In addition, cloud radiative feedbacks shaped some but not all tropical SST responses. Notably, shared equatorial Pacific and Atlantic and western Indian Ocean responses for both 2 × CO$_2$ and 0.5 × CO$_2$ including associated wind changes were unaffected by cloud locking (Figs. 15a,b). In addition, cloud influence on
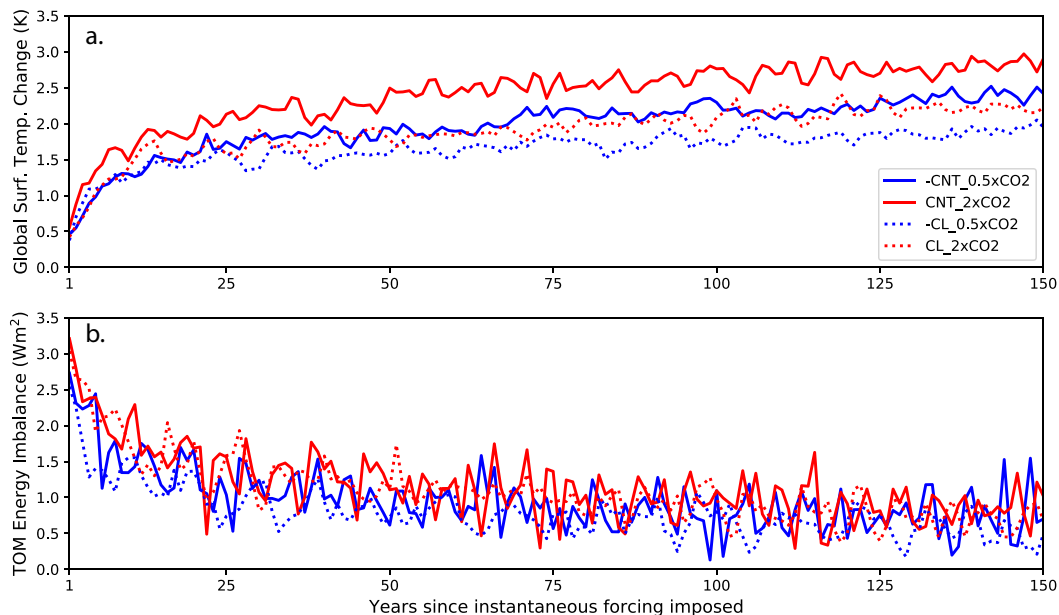

FIG. 12. Global surface temperature and top of model energy imbalance time evolution for simulations with (CNT_2×CO2, CNT_0.5×CO2) and without cloud radiative feedbacks (CL_2×CO2, CL_0.5×CO2).
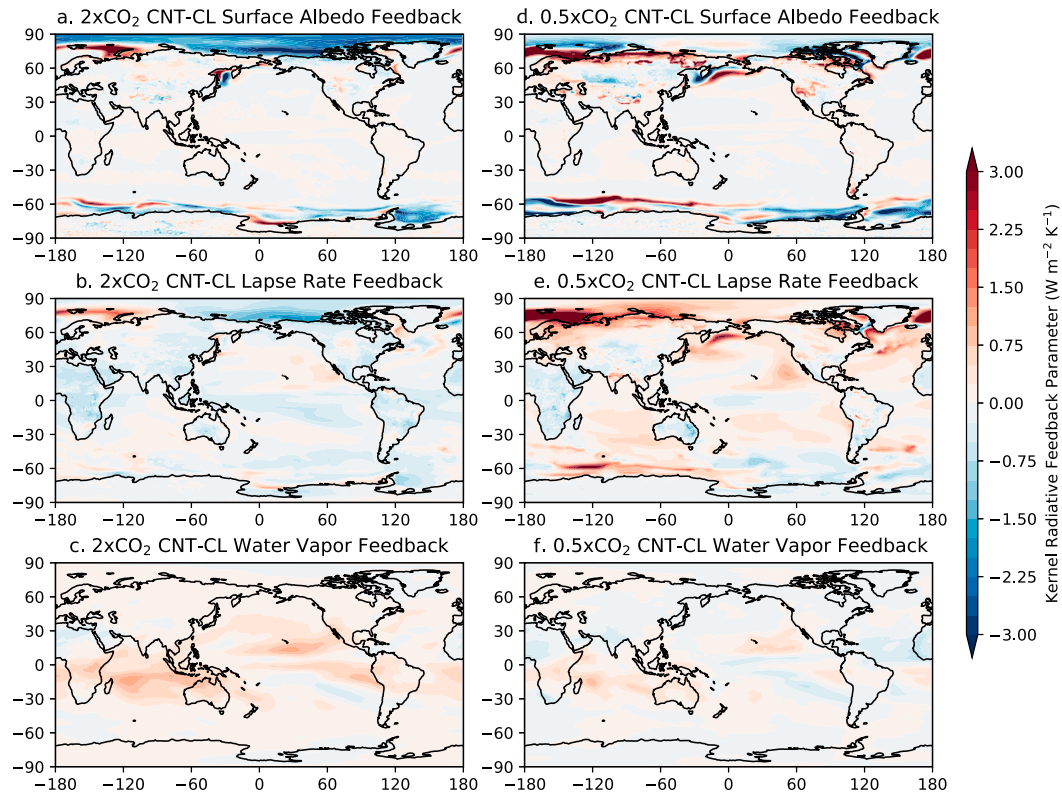
FIG. 13. Cloud influence on non-cloud feedbacks: (a) $2 \times CO_2$ surface albedo; (b) $2 \times CO_2$ lapse rate; (c) $2 \times CO_2$ water vapor; and (d)–(f) as in (a)–(c), but for $0.5 \times CO_2$. All feedbacks are calculated using radiative kernels for years 100–150. All feedbacks are normalized by the global mean temperature. Cloud influence is calculated by differencing simulations with and without cloud radiative feedbacks (CNT-CL).

the Indian and tropical Atlantic Ocean was generally small, especially for the slow response (Fig. 16). But, enabling cloud radiative feedbacks increased the western tropical Pacific SST response, especially for $2 \times CO_2$ (Figs. 15c,d). This cloud influence on the western tropical Pacific was fast and largely occurred in the first 50 years (Fig. 16). Cloud influence also created asymmetry across the equatorial Pacific with a larger response in the Northern Hemisphere than in Southern
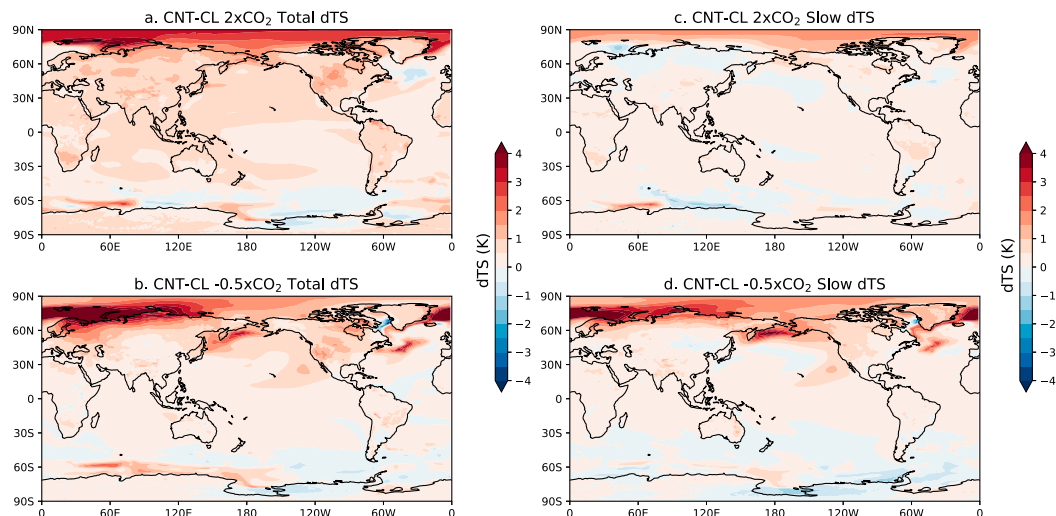

FIG. 14. Global maps of cloud influence on the total and the slow surface temperature change (dTS). Cloud influence is calculated by differencing simulations with and without cloud radiative feedbacks (CNT-CL). The slow change is the total change (average over years 100–150) minus the fast (average over years 1–50) change.
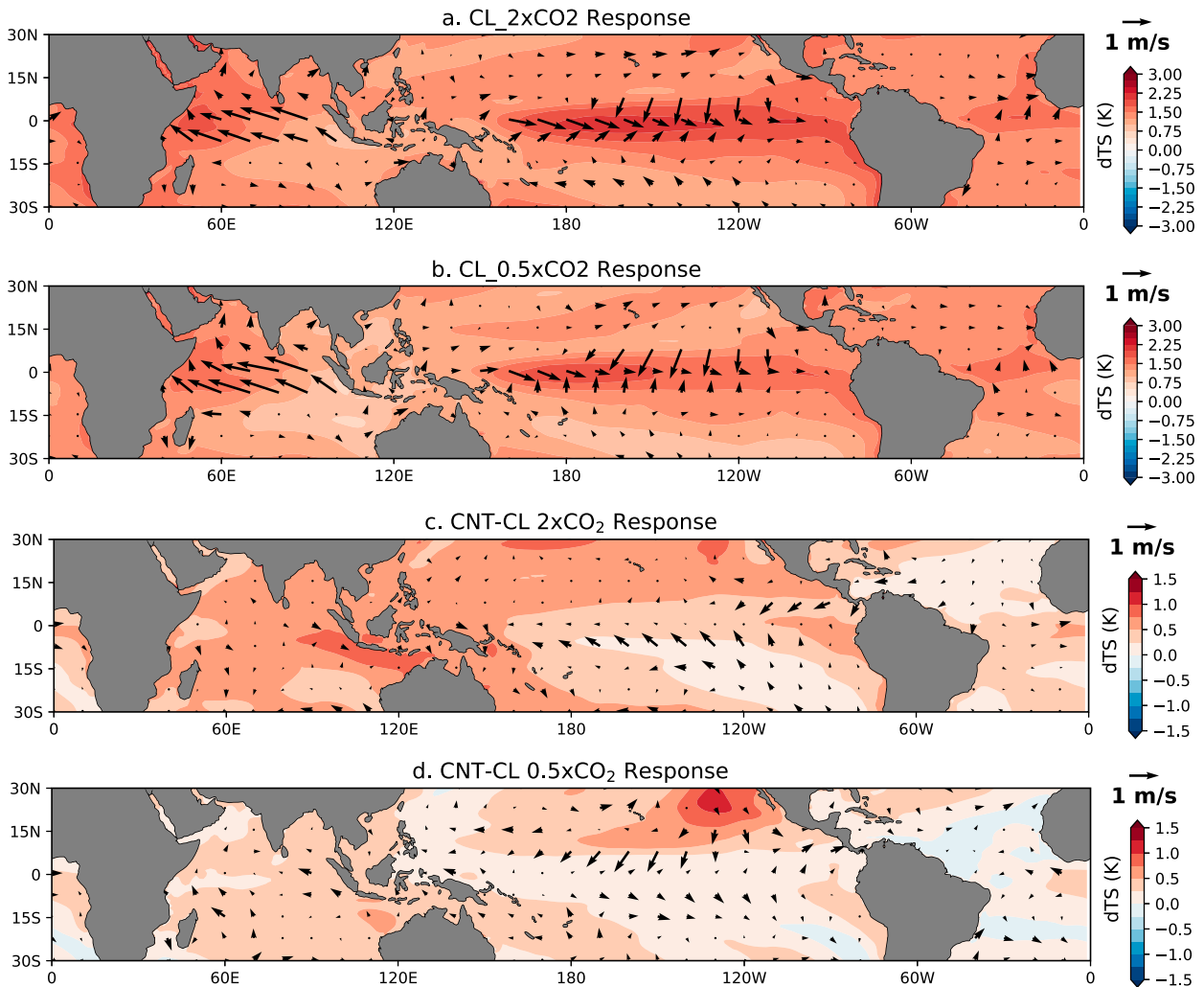
FIG. 15. Tropical ocean total response (average over years 100–150): (a) $2 \times CO_2$ without cloud radiative feedbacks (CL_$2 \times CO_2$) surface temperature change (colors) and surface wind changes (black arrows); (b) as in (a), but for $0.5 \times CO_2$, (c) as in (a), but $2 \times CO_2$ cloud influence; and (d) as in (a), but $0.5 \times CO_2$ cloud influence. Cloud influence is calculated by differencing simulations with and without cloud radiative feedbacks (CNT-CL). Note that in (c) and (d) dTS color contours are scaled at half of (a) and (b).

Hemisphere (Figs. 15c,d). This asymmetry resulted from enhanced $2 \times CO_2$ warming across the entire northern tropical Pacific, but enhanced $0.5 \times CO_2$ cooling only in the northeastern tropical Pacific. While the cloud influence on the zonally uniform $2 \times CO_2$ north tropical Pacific warming was fast, the cloud influence on the northeastern tropical Pacific cooling was slow (Fig. 16), and potentially connected to the slow North Pacific cooling (Fig. 8). There was also delayed response in the southeastern tropical Pacific.

With the equal-but-opposite responses removed, the amplitude and pattern of tropical ocean differences between $2 \times CO_2$ and $0.5 \times CO_2$ were strongly affected by cloud radiative feedbacks (Fig. 17). Cloud influence doubled the magnitude of tropical ocean response differences between $2 \times CO_2$ and $0.5 \times CO_2$ in many regions including the Indian Ocean, the west Pacific, the equatorial Pacific, and the South Atlantic. Cloud influence created asymmetry across the equator in the

tropical ocean response differences between $2 \times CO_2$ and $0.5 \times CO_2$. In contrast, surface wind differences between $2 \times CO_2$ and $0.5 \times CO_2$ were modest.

4. Discussion

The most important result found in this study is that the cloud influence on idealized greenhouse warming and cooling goes well beyond local cloud radiative feedbacks. Enabling cloud radiative feedbacks increases effective radiative forcing and amplifies the surface temperature response almost everywhere. Remarkably, cloud feedbacks diagnosed offline have only modest pattern correspondence with the cloud influence found by differencing experiments with and without cloud radiative feedbacks. By coupling with the circulation and noncloud feedbacks, clouds amplify the response pattern, even where local cloud radiative feedbacks are small. Cloud
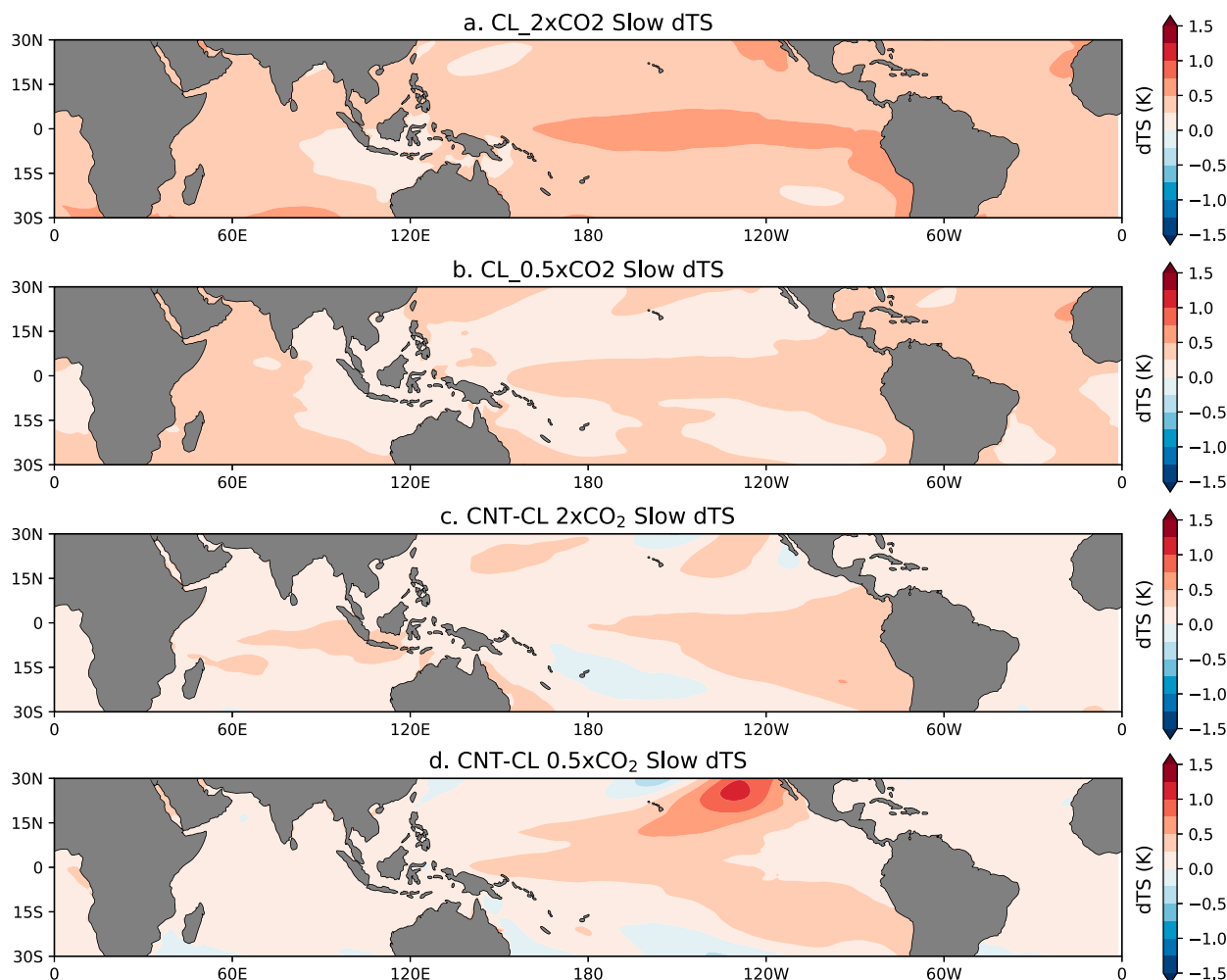
FIG. 16. Tropical ocean slow change in surface temperature: (a) $2 \times CO_2$ without cloud radiative feedbacks (CL_$2\times CO_2$), (b) $0.5 \times CO_2$ without cloud radiative feedbacks (CL_$0.5\times CO_2$), (c) $2 \times CO_2$ cloud influence, and (d) $0.5 \times CO_2$ cloud influence. The slow change is the total change (average over years 100–150) minus the fast change (average over years 1–50).

influence on non-cloud feedback is also state dependent. For example, cloud influence on tropical water vapor feedbacks is larger for $2 \times CO_2$ than for $0.5 \times CO_2$. Clouds having effects well beyond those diagnosed with local feedback analysis is consistent with Middlemas et al. (2020) who found Arctic warming was more strongly affected by disabling global cloud feedback than disabling local Arctic cloud feedbacks. The results are also consistent with Chen et al. (2021) who diagnose mechanisms for interhemisphere differences in cloud coupling with circulation. The work adds to a large body of literature showing cloud coupling with circulation and with non-cloud feedbacks is needed to fully understand cloud influence on the climate system (e.g., Chen et al. 2021; Middlemas et al. 2020; Middlemas et al. 2019; Zhou et al. 2017; Mauritsen et al. 2013).

The tropical Pacific is unique because its response patterns are shaped by local cloud radiative feedbacks. Indeed, cloud feedbacks control some but not all aspects of the pattern and time evolution of the tropical Pacific SST response to $2 \times$ CO_2 and $0.5 \times CO_2$. Since many aspects of the tropical Pacific response to $2 \times CO_2$ and $0.5 \times CO_2$ were nearly equal but opposite, $2 \times CO_2 - 0.5 \times CO_2$ cloud feedback differences were especially important for explaining $2 \times CO_2 - (-0.5 \times CO_2)$ SST response differences. Consistent with previous multimodel analysis of greenhouse warming that diagnose cloud feedbacks (Dong et al. 2020; Andrews et al. 2015), we find enabling cloud feedbacks amplifies the fast western tropical Pacific response and the slow eastern tropical Pacific responses. That clouds affect the east–west gradient across the Pacific including its temporal evolution is intriguing. Yet, we expect the spatial pattern and magnitude of this cloud influence are very likely model dependent, especially in the eastern subtropical Pacific where there are large biases in low cloud cover and shortwave cloud forcing in CESM1-CAM5 (e.g., Kay et al. 2012) and large multimodel differences in cloud radiative effects (e.g., DiNezio et al. 2009).

The high-latitude ocean surface temperature response and associated feedbacks are strongly shaped by sea ice with
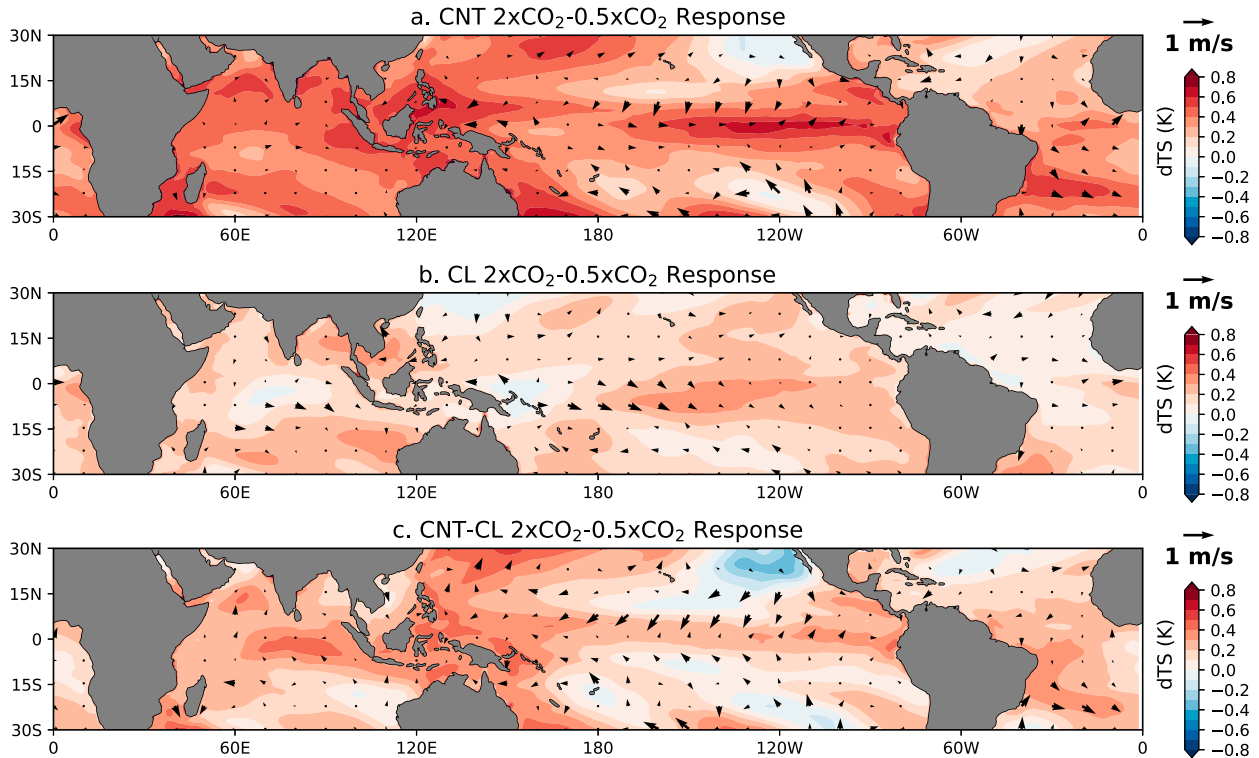
FIG. 17. Tropical maps of $2 \times CO_2 - 0.5 \times CO_2$ surface temperature (color) and surface wind (black arrow) response: (a) with cloud feedbacks (CNT_2×CO$_2$ − CNT_ 0.5×CO$_2$), (b) without cloud feedbacks (CL_2×CO$_2$ − CL_0.5×CO$_2$), and (c) cloud influence on $2 \times CO_2 - 0.5 \times CO_2$ difference. Cloud influence is calculated by differencing simulations with and without cloud radiative feedbacks (CNT-CL).

striking differences in their time evolution. Delayed Southern Ocean warming is a well-known feature of greenhouse warming (Manabe et al. 1990) that results from the uptake of heat by the mean overturning circulation (Armour et al. 2016). Yet unlike the relatively slow $2 \times CO_2$ warming over the Southern Ocean in our 150-yr-long experiments, Southern Ocean $0.5 \times CO_2$ is relatively fast. Why is the Southern Ocean cooling happening so quickly? Covering the Southern Ocean with sea ice under global cooling decreases air-sea fluxes and thus removes the ocean circulation response buffer in a key region (Stouffer and Manabe 2003). This asymmetry in ocean buffering leads to asymmetries in carbon and heat exchanges under global warming and cooling over the Southern Ocean. Indeed, covering the Southern Ocean with sea ice severely limits air–sea fluxes in a primary region of deep water ventilation (Stephens and Keeling 2000). Reduction in the exchanges of surface and deep water has profound implications for ice age climates (Sigman et al. 2021). Future work could examine asymmetries in westerly wind changes and their influence on surface ocean carbon dioxide in these simulations (Toggweiler et al. 2006). This work is of particular interest since CESM1-CAM5 has a realistic present-day Southern Hemisphere mid-latitude jet position that shifts less in response to forcing than other models of its class (Kay et al. 2014; Barnes and Polvani 2013).

In contrast, high northern latitude ocean $2 \times CO_2$ warming is much faster than $0.5 \times CO_2$ cooling. The corresponding slower pace of Northern Hemisphere sea ice advance under global cooling than sea ice retreat under global warming is also striking. Indeed, the continued advance of sea ice throughout all 150 years of the global cooling experiments creates delayed surface cooling over the North Atlantic and Pacific and increasingly positive lapse rate feedbacks there. Enabling cloud feedbacks enhances this phenomenon. These increasingly positive $0.5 \times CO_2$ lapse rate feedbacks contribute to global $2 \times CO_2 - 0.5 \times CO_2$ lapse rate feedback differences that oppose global $2 \times CO_2 - 0.5 \times CO_2$ shortwave cloud feedbacks differences. In the North Pacific, this cooling and sea ice advance may affect cloud feedbacks at latitudes via the wind–evaporation–SST feedback. It could help explain some of the $2 \times CO_2 - 0.5 \times CO_2$ response asymmetry in the eastern tropical Pacific cloud feedbacks. More generally, these results raise questions about how the interlinked positive surface albedo and lapse rate feedbacks change as the sea ice change moves to lower latitudes with differing insolation, stratification, and ocean circulation. A more detailed assessment of the coupled processes associated with the ice edge moving meridionally in fully coupled models including assessment of cloud influence is recommended for future work. Such an assessment could also take advantage of new

methods to separate the surface and atmospheric heat transport contributions to lapse rate feedbacks (Feldl et al. 2020).

Our idealized results inform debate on paleoclimate constraints on future warming. According to a recent synthesis by Sherwood et al. (2020), the amount of global cooling during the LGM provides the tightest constraint on the upper bound of equilibrium future warming. Specifically, Sherwood et al. (2020) argue the LGM cooling provides strong evidence against the largest values of equilibrium climate sensitivity (4.5+ K). That said, if state-dependent feedbacks lead to substantially more global warming than global cooling, as found here, the LGM constraint on the upper bound of ECS increases (Tierney et al. 2020). While the existence of climate state dependence has been well documented in models for decades, its magnitude and underlying process controls still remain uncertain. Three points are important to emphasize here. First, to credibly argue that the largest values of equilibrium climate sensitivity (i.e., 4.5+ K) are consistent with LGM cooling, larger asymmetries controlling global cooling and warming than those that are found here are needed. For example, combining the 20% asymmetry found here with the Tierney et al. (2020) LGM-informed ECS estimate of 3.4 K puts an upper limit on ECS of 4.08 K. Second clouds are an important and well-known source of state-dependent feedbacks. Yet here we find more global warming than global cooling occurs even when cloud radiative feedbacks are disabled.

There are two notable limitations to this work. First, with simulation lengths of only 150 years our experiments are many centuries away from their fully equilibrated response (Rugenstein et al. 2020, Stouffer 2004). Thus, the results here are mostly relevant for fast feedbacks and upper ocean processes. The equilibrium surface temperature response to a CO_2 doubling in CESM1-CAM5 estimated using a slab ocean model is 4.0 K (Gettelman et al. 2012). Over the last 50 years of our $2 \times CO_2$ simulation, the globe warmed by 2.75 K or ~70% of the total anticipated surface temperature response. While understanding this initial response is certainly of value, the equilibrium response will likely differ, especially in regions whose responses are strongly shaped by ocean circulation. For example, the initial AMOC response of weakening under $2 \times CO_2$ and strengthening under $0.5 \times CO_2$ in our experiments is consistent with initial responses seen in other models (Stouffer and Manabe 2003). Yet, when other model simulations were run out for thousands of years, it became clear that the equilibrated AMOC response cannot be inferred from the initial AMOC response (Stouffer and Manabe 2003; Jansen et al. 2018).

Second, we use one model: CESM1-CAM5. Notably, this model is fully coupled and run at the standard resolution used for historical and future projections. The model has been extensively used and is a top-performing CMIP5 model when evaluated against modern (Knutti et al. 2013; Kay et al. 2012) and paleoclimate (Zhu and Poulsen 2021; Zhu et al. 2019; DiNezio et al. 2018) constraints. We encourage more simulations with cloud radiative feedbacks disabled to assess the robustness of the results here. But we acknowledge the cloud locking experiments analyzed here are not easily reproduced

in multiple models. Disabling cloud radiative feedbacks requires running new simulations and a vetted implementation of cloud locking (e.g., Middlemas et al. 2019). Comparison of the fully coupled results here with similar experiments that are part of CMIP6 (Webb et al. 2017) could help reveal aspects of the responses found here that are model dependent.

5. Summary and conclusions

Examining abrupt CO_2 forcing simulations with a global fully coupled climate model CESM1-CAM5, we found the following:

- After 150 years, there was 20% more $2 \times CO_2$ global warming than $0.5 \times CO_2$ global cooling. This difference resulted from 1) ~10% larger effective radiative forcing (ERF) for $2 \times CO_2$ than for $0.5 \times CO_2$ and 2) less negative radiative feedbacks for $2 \times CO_2$ than for $0.5 \times CO_2$ due largely to positive shortwave cloud feedbacks, with some opposition by lapse rate feedbacks.
- Over high-latitude oceans, $2 \times CO_2 - (-0.5 \times CO_2)$ surface temperature response differences were amplified by linked positive surface albedo and lapse rate feedbacks associated with sea ice change. While $2 \times CO_2$ warming was faster than $0.5 \times CO_2$ cooling at high northern latitudes, $0.5 \times CO_2$ cooling was faster than $2 \times CO_2$ warming at high southern latitudes.
- At low latitudes, $2 \times CO_2$ warming exceeded $0.5 \times CO_2$ cooling almost everywhere due to both larger $2 \times CO_2$ forcing and more positive $2 \times CO_2$ shortwave cloud feedbacks. Tropical Pacific cloud feedback patterns amplify 1) more fast $2 \times CO_2$ warming than fast $0.5 \times CO_2$ cooling in the west and 2) slow $2 \times CO_2 - (-0.5 \times CO_2)$ pattern differences in the east.
- Disabling cloud radiative feedbacks reduced ERF and resulted in less global warming and less global cooling.
- Regardless of whether cloud feedbacks were enabled or disabled, global warming exceeded global cooling by 20%. This surprising consistency in the asymmetry between global warming and cooling resulted from the cloud influence on non-cloud feedbacks.
- The cloud influence on climate response diagnosed by comparing simulations with and without cloud radiative feedbacks is much greater than those solely attributable local cloud radiative effects. Disabling cloud feedbacks strongly affected climate responses in regions with small cloud feedbacks, notably the high latitudes.
- Disabling cloud feedbacks did not affect surface temperature response patterns. A notable exception is the tropical Pacific where cloud feedbacks shaped the pattern and time evolution of the SST response.

Moving forward, these results provide new perspectives on the processes driving differences between idealized greenhouse warming and cooling especially for clouds. While we document and explain many interesting patterns and their time evolution using novel and state-of-the-art techniques, much more could be done. For example, how do atmosphere

and ocean circulation respond to and interact with disabled cloud feedbacks? What are the implications of the non-equal-but-opposite responses shown here for carbon cycle feedbacks? How do hemispheric differences in the time and spatial pattern evolution of warming and cooling interact with feedbacks? Understanding the regional processes that drive nonlinear responses to global warming and cooling remains a rich research area with important consequences for future climate projections and forcing.

REFERENCES

Alexander, M., I. Bladé, M. Newman, J. R. Lanzante, N.-C. Lau, and J. D. Scott, 2002: The atmospheric bridge: The influence of ENSO teleconnections on air-sea interaction over the global oceans. *J. Climate.*, **15**, 2205–2228, https://doi.org/10.1175/1520-0442(2002)015<2205:TABTIO>2.0.CO;2.

Andrews, T., J. M. Gregory, P. M. Forster, and M. J. Webb, 2011: Cloud adjustment and its role in CO_2 radiative forcing and climate sensitivity: A review. *Surv. Geophys.*, **41**, 287–303, https://doi.org/10.1007/978-94-007-4327-4_19.

——, ——, and M. J. Webb, 2015: The dependence of radiative forcing and feedback on evolving patterns of surface temperature change in climate models. *J. Climate*, **28**, 1630–1648, https://doi.org/10.1175/JCLI-D-14-00545.1.

Armour, K. C., J. Marshall, J. R. Scott, A. Donohoe, and E. R. Newsom, 2016: Southern Ocean warming delayed by circumpolar upwelling and equatorward transport. *Nat. Geosci.*, **9**, 549–554, https://doi.org/10.1038/ngeo2731.

Barnes, E. A., and L. M. Polvani, 2013: Response of the midlatitude jets and of their variability to increased greenhouse gases in the CMIP5 models. *J. Climate*, **26**, 7117–7135, https://doi.org/10.1175/JCLI-D-12-00536.1.

Bloch-Johnson, J., M. Rugenstein, M. B. Stolpe, T. Rohrschneider, Y. Zheng, and J. M. Gregory, 2020: Climate sensitivity increases under higher CO_2 levels due to feedback temperature

dependence. *Geophys. Res. Lett.*, **48**, e2020GL089074, https://doi.org/10.1029/2020GL089074.

Boucher, O., and Coauthors, 2013: Clouds and aerosols. *Climate Change 2013: The Physical Science Basis*, T. F. Stocker et al., Eds., Cambridge University Press, 571–657, https://doi.org/10.1017/CBO9781107415324.016.

Byrne, B., and C. Goldblatt, 2014: Radiative forcing at high concentrations of well-mixed greenhouse gases. *Geophys. Res. Lett.*, **41**, 152–160, https://doi.org/10.1002/2013GL058456.

Byrne, M. P., and P. O'Gorman, 2018: Trends in continental temperature and humidity directly linked to ocean warming. *Proc. Natl. Acad. Sci. USA*, **115**, 4863–4868, https://doi.org/10.1073/pnas.1722312115.

Caballero, R., and M. Huber, 2013: State-dependent climate sensitivity in past warm climates and its implications for future climate projections. *Proc. Natl. Acad. Sci. USA*, **110**, 14162–14167, https://doi.org/10.1073/pnas.1303365110.

Chen, Y.-J., Y. T. Hwang, and P. Ceppi, 2021: The impacts of cloud-radiative changes on poleward atmospheric and oceanic energy transport in a warmer climate. *J. Climate*, **34**, 7857–7874, https://doi.org/10.1175/JCLI-D-20-0949.1.

Colman, R., and B. McAvaney, 1997: A study of general circulation model climate feedbacks determined from perturbed sea surface temperature experiments. *J. Geophys. Res.*, **102**, 19383–19402, https://doi.org/10.1029/97JD00206.

——, and ——, 2009: Climate feedbacks under a very broad range of forcing. *Geophys. Res. Lett.*, **36**, L01702, https://doi.org/10.1029/2008GL036268.

Deng, J., A. Dai, and H. Xu, 2020: Nonlinear climate responses to increasing CO_2 and anthropogenic aerosols simulated by CESM1. *J. Climate*, **33**, 281–301, https://doi.org/10.1175/JCLI-D-19-0195.1.

DiNezio, P. N., A. C. Clement, G. A. Vecchi, B. J. Soden, B. P. Kirtman, and S. K. Lee, 2009: Climate response of the equatorial Pacific to global warming. *J. Climate*, **22**, 4873–4892, https://doi.org/10.1175/2009JCLI2982.1.

——, J. E. Tierney, B. L. Otto-Bliesner, A. Timmermann, T. Bhattacharya, N. Rosenbloom, and E. Brady, 2018: Glacial changes in tropical climate amplified by the Indian Ocean. *Sci. Adv.*, **4**, eaat9658, https://doi.org/10.1126/sciadv.aat9658.

Dong, Y., K. C. Armour, M. D. Zelinka, C. Proistosescu, D. S. Battisti, C. Zhou, and T. Andrews, 2020: Intermodel spread in the pattern effect and its contribution to climate sensitivity in CMIP5 and CMIP6 models. *J. Climate*, **33**, 7755–7775, https://doi.org/10.1175/JCLI-D-19-1011.1.

Etminan, M., G. Myhre, E. J. Highwood, and K. P. Shine, 2016: Radiative forcing of carbon dioxide, methane, and nitrous oxide: A significant revision of the methane radiative forcing. *Geophys. Res. Lett.*, **43**, 12614–12623, https://doi.org/10.1002/2016GL071930.

Feldl, N., S. Po-Chedley, H. K. A. Singh, S. Hay, and P. J. Kushner, 2020: Sea ice and atmospheric circulation shape the high-latitude lapse rate feedback. *npj Climate Atmos. Sci.*, **3**, 41, https://doi.org/10.1038/s41612-020-00146-7.

Forster, P. M., and Coauthors, 2016: Recommendations for diagnosing effective radiative forcing from climate models for CMIP6. *J. Geophys. Res. Atmos.*, **121**, 12460–12475, https://doi.org/10.1002/2016JD025320.

Frey, W. R., and J. E. Kay, 2018: The influence of extratropical cloud phase and amount feedbacks on climate sensitivity. *Climate Dyn.*, **50**, 3097–3116, https://doi.org/10.1007/s00382-017-3796-5.

Gettelman, A., J. E. Kay, and K. Shell, 2012: The evolution of climate sensitivity and climate feedbacks in the Community Atmosphere Model. *J. Climate*, **25**, 1453–1469, https://doi.org/10.1175/JCLI-D-11-00197.1.

Gregory, J. M., and Coauthors, 2004: A new method for diagnosing radiative forcing and climate sensitivity. *Geophys. Res. Lett.*, **31**, L03205, https://doi.org/10.1029/2003GL018747.

——, T. Andrews, and P. Good, 2015: The inconstancy of the transient climate response parameter under increasing CO_2. *Philos. Trans. Roy. Soc. London*, **373A**, 20140417, https://doi.org/10.1098/rsta.2014.0417.

Grise, K. M., B. Medeiros, J. J. Benedict, and J. G. Olson, 2019: Investigating the influence of cloud radiative effects on the extratropical storm tracks. *Geophys. Res. Lett.*, **46**, 7700–7707, https://doi.org/10.1029/2019GL083542.

Hansen, J., and Coauthors, 2005: Efficacy of climate forcings. *J. Geophys. Res.*, **110**, D18104, https://doi.org/10.1029/2005JD005776.

Hurrell, J. W., and Coauthors, 2013: The Community Earth System Model: A framework for collaborative research. *Bull. Amer. Meteor. Soc.*, **94**, 1339–1360, https://doi.org/10.1175/BAMS-D-12-00121.1.

Iacono, M. J., J. S. Delamere, E. J. Mlawer, M. W. Shephard, S. A. Clough, and W. D. Collins, 2008: Radiative forcing by long-lived greenhouse gases: Calculations with the AER radiative transfer models. *J. Geophys. Res.*, **113**, D13103, https://doi.org/10.1029/2008JD009944.

Ihara, C., Y. Kushnir, M. A. Cane, and V. H. de la Peña, 2009: Climate change over the equatorial Indo-Pacific in global warming. *J. Climate*, **22**, 2678–2693, https://doi.org/10.1175/2008JCLI2581.1.

Jansen, M. F., L. P. Nadeau, and T. M. Merlis, 2018: Transient versus equilibrium response of the ocean's overturning circulation to warming. *J. Climate*, **31**, 5147–5163, https://doi.org/10.1175/JCLI-D-17-0797.1.

Jonko, A. K., K. M. Shell, B. M. Sanderson, and G. Danabasoglu, 2013: Climate feedbacks in CCSM3 under changing CO_2 forcing. Part II: Variation of climate feedbacks and sensitivity with forcing. *J. Climate*, **26**, 2784–2795, https://doi.org/10.1175/JCLI-D-12-00479.1.

Kay, J. E., and Coauthors, 2012: Exposing global cloud biases in the Community Atmosphere Model (CAM) using satellite observations and their corresponding instrument simulators. *J. Climate*, **25**, 5190–5207, https://doi.org/10.1175/JCLI-D-11-00469.1.

——, B. Medeiros, Y.-T. Hwang, A. Gettelman, J. Perket, and M. G. Flanner, 2014: Processes controlling Southern Ocean shortwave climate feedbacks in CESM. *Geophys. Res. Lett.*, **41**, 616–622, https://doi.org/10.1002/2013GL058315.

——, and Coauthors, 2015: The Community Earth System Model (CESM) large ensemble project: A community resource for studying climate change in the presence of internal climate variability. *Bull. Amer. Meteor. Soc.*, **96**, 1333–1349, https://doi.org/10.1175/BAMS-D-13-00255.1.

Knutti, R., D. Masson, and A. Gettelman, 2013: Climate model genealogy: Generation CMIP5 and how we got there. *Geophys. Res. Lett.*, **40**, 1194–1199, https://doi.org/10.1002/grl.50256.

Kutzbach, J. E., F. He, S. J. Vavrus, and W. F. Ruddiman, 2013: The dependence of equilibrium climate sensitivity on climate state: Applications to studies of climates colder than present. *Geophys. Res. Lett.*, **40**, 3721–3726, https://doi.org/10.1002/grl.50724.

Manabe, S., and R. T. Wetherald, 1967: Thermal equilibrium of the atmosphere with a given distribution of relative humidity. *J. Atmos. Sci.*, **24**, 241–259, https://doi.org/10.1175/1520-0469(1967)024<0241:TEOTAW>2.0.CO;2.

——, and R. J. Stouffer, 1980: Sensitivity of a global climate model to an increase of CO_2 concentration in the atmosphere. *J. Geophys. Res.*, **85**, 5529–5554, https://doi.org/10.1029/JC085iC10p05529.

——, and K. Bryan, 1985: CO_2-induced change in a coupled ocean-atmosphere model and its paleoclimatic implications. *J. Geophys. Res.*, **90**, 11 689–11 707, https://doi.org/10.1029/JC090iC06p11689.

——, ——, and M. J. Spelman, 1990: Transient response of a global ocean–atmosphere model to a doubling of atmospheric carbon dioxide. *J. Phys. Oceanogr.*, **20**, 722–749, https://doi.org/10.1175/1520-0485(1990)020<0722:TROAGO>2.0.CO;2.

Mauritsen, T., R. G. Graversen, D. Klocke, P. L. Langen, B. Stevens, and L. Tomassini, 2013: Climate feedback efficiency and synergy. *Climate Dyn.*, **41**, 2539–2554, https://doi.org/10.1007/s00382-013-1808-7.

Meehl, G. A., and W. M. Washington, 1996: El Niño-like climate change in a model with increased atmospheric CO_2 concentrations. *Nature*, **382**, 56–60, https://doi.org/10.1038/382056a0.

Meehl, G., and Coauthors, 2013: Climate change projections in CESM1(CAM5) compared to CCSM4. *J. Climate*, **26**, 6287–6308, https://doi.org/10.1175/JCLI-D-12-00572.1.

Meraner, K., T. Mauritsen, and A. Voigt, 2013: Robust increase in equilibrium climate sensitivity under global warming. *Geophys. Res. Lett.*, **40**, 5944–5948, https://doi.org/10.1002/2013GL058118.

Middlemas, E. A., A. C. Clement, B. Medeiros, and B. Kirtman, 2019: Cloud radiative feedbacks and El Niño–Southern Oscillation. *J. Climate*, **32**, 4661–4680, https://doi.org/10.1175/JCLI-D-18-0842.1.

——, J. E. Kay, B. M. Medeiros, and E. A. Maroon, 2020: Quantifying the influence of cloud radiative feedbacks on Arctic surface warming using cloud locking in an earth system model. *Geophys. Res. Lett.*, **47**, e2020GL089207, https://doi.org/10.1029/2020GL089207.

Mitevski, I., C. Orbe, R. Chemke, L. Nazarenko, and L. M. Polvani, 2021: Non-monotonic response of the climate system to abrupt CO_2 forcing. *Geophys. Res. Lett.*, **48**, e2020GL090861, https://doi.org/10.1029/2020GL090861.

Morrison, A. L., J. E. Kay, W. R. Frey, H. Chepfer, and R. Guzman, 2019: Cloud response to Arctic Sea ice loss and implications for future feedbacks in the CESM1 climate model. *J. Geophys. Res. Atmos.*, **124**, 1003–1020, https://doi.org/10.1029/2018JD029142.

Myers, T. A., R. C. Scott, M. D. Zelinka, S. A. Klein, J. R. Norris, and P. M. Caldwell, 2021: Observational constraints on low cloud feedback reduce uncertainty of climate sensitivity. *Nat. Climate Change*, **11**, 501–507, https://doi.org/10.1038/s41558-021-01039-0.

Myhre, G., E. J. Highwood, K. P. Shine, and F. Stordal, 1998: New estimates of radiative forcing due to well mixed greenhouse gases. *Geophys. Res. Lett.*, **25**, 2715–2718, https://doi.org/10.1029/98GL01908.

Pendergrass, A. G., A. Conley, and F. M. Vitt, 2018: Surface and top-of-atmosphere radiative feedback kernels for CESM-CAM5. *Earth System Data*, **10**, 317–324, https://doi.org/10.5194/essd-10-317-2018.

Rugenstein, M., and Coauthors, 2020: Equilibrium climate sensitivity estimated by equilibrating climate models.

Geophys. Res. Lett., **47**, e2019GL083898, https://doi.org/10.1029/2019GL083898.

Shell, K. M., J. T. Kiehl, and C. A. Shields, 2008: Using the radiative kernel technique to calculate climate feedbacks in NCAR's Community Atmospheric Model. *J. Climate*, **21**, 2269–2282, https://doi.org/10.1175/2007JCLI2044.1.

Sherwood, S., M. J. Webb, J. D. Annan, K. C. Armour, P. M. Forster, J. C. Hargreaves, and M. D. Zelinka, 2020: An assessment of Earth's climate sensitivity using multiple lines of evidence. *Rev. Geophys.*, **58**, e2019RG000678, https://doi.org/10.1029/2019RG000678..

Sigman, D. M., and Coauthors, 2021: The Southern Ocean during the ice ages: A review of the Antarctic surface isolation hypothesis, with comparison to the North Pacific. *Quat. Sci. Rev.*, **254**, 106732, https://doi.org/10.1016/j.quascirev.2020.106732.

Soden, B. J., I. M. Held, R. Colman, K. M. Shell, J. T. Kiehl, and C. A. Shields, 2008: Quantifying climate feedbacks using radiative kernels. *J. Climate*, **21**, 3504–3520, https://doi.org/10.1175/2007JCLI2110.1.

Stephens, B. B., and R. F. Keeling, 2000: The influence of Antarctic sea ice on glacial–interglacial CO_2 variations. *Nature*, **404**, 171–174, https://doi.org/10.1038/35004556.

Stouffer, R., 2004: Time scales of climate response. *J. Climate*, **17**, 209–217, https://doi.org/10.1175/1520-0442(2004)017<0209:TSOCR>2.0.CO;2.

——, and S. Manabe, 2003: Equilibrium response of thermohaline circulation to large changes in atmospheric CO_2 concentration. *Climate Dyn.*, **20**, 759–773, https://doi.org/10.1007/s00382-002-0302-4.

Sutton, R. T., B. Dong, and J. M. Gregory, 2007: Land/sea warming ratio in response to climate change: IPCC AR4 model results and comparison with observations. *Geophys. Res. Lett.*, **34**, L02701, https://doi.org/10.1029/2006GL028164.

Taylor, K. E., M. Crucifix, P. Braconnot, C. D. Hewitt, C. Doutriaux, A. J. Broccoli, J. F. B. Mitchell, and M. J. Webb, 2007: Estimating shortwave radiative forcing and response in climate models. *J. Climate*, **20**, 2530–2543, https://doi.org/10.1175/JCLI4143.1.

Tierney, J. E., J. Zhu, J. King, S. B. Malevich, G. J. Hakim, and C. J. Poulsen, 2020: Glacial cooling and climate sensitivity revisited. *Nature*, **584**, 569–573, https://doi.org/10.1038/s41586-020-2617-x.

Toggweiler, J. R., J. L. Russell, and C. R. Carson, 2006: Midlatitude westerlies, atmospheric CO_2, and climate change during the ice ages. *Paleoceanography*, **21**, PA2005, https://doi.org/10.1029/2005PA001154.

Vecchi, G. A., and B. J. Soden, 2007: Global warming and the weakening of the tropical circulation. *J. Climate*, **20**, 4316–4340, https://doi.org/10.1175/JCLI4258.1.

Webb, M. J., and Coauthors, 2017: The Cloud Feedback Model Intercomparison Project (CFMIP) contribution to CMIP6. *Geosci. Model Dev.*, **10**, 359–384, https://doi.org/10.5194/gmd-10-359-2017.

Xie, S. P., C. Deser, G. A. Vecchi, J. Ma, H. Teng, and A. Wittenberg, 2010: Global warming pattern formation: Sea surface temperature and rainfall. *J. Climate*, **23**, 966–986, https://doi.org/10.1175/2009JCLI3329.1.

Yoshimori, M., T. Yokohata, and A. A. Abe-Ouchi, 2009: A comparison of climate feedback strength between CO_2 doubling and LGM experiments. *J. Climate*, **22**, 3374–3395, https://doi.org/10.1175/2009JCLI2801.1.

Zelinka, M. D., D. A. Randall, M. J. Webb, and S. A. Klein, 2017: Clearing clouds of uncertainty. *Nat. Climate Change*, **7**, 674–678, https://doi.org/10.1038/nclimate3402.

Zhang, M. H., J. J. Hack, J. T. Kiehl, and R. D. Cess, 1994: Diagnostic study of climate feedback processes in atmospheric general circulation models. *J. Geophys. Res.*, **99**, 5525–5537, https://doi.org/10.1029/93JD03523.

Zhou, C., M. D. Zelinka, and S. A. Klein, 2017: Analyzing the dependence of global cloud feedback on the spatial pattern of sea surface temperature change with a Green's function approach. *J. Adv. Model. Earth Syst.*, **9**, 2174–2189, https://doi.org/10.1002/2017MS001096.

Zhu, J., and C. J. Poulsen, 2020: On the increase of climate sensitivity and cloud feedback with warming in the community atmosphere models. *Geophys. Res. Lett.*, **47**, e2020GL089143, https://doi.org/10.1029/2020GL089143.

——, and ——, 2021: Last Glacial Maximum (LGM) climate forcing and ocean dynamical feedback and their implications for estimating climate sensitivity. *Climate Past*, **17**, 253–267, https://doi.org/10.5194/cp-17-253-2021.

——, ——, and J. E. Tierney, 2019: Simulation of Eocene extreme warmth and high climate sensitivity through cloud feedbacks. *Sci. Adv.*, **5**, eaax1874, https://doi.org/10.1126/sciadv.aax1874.

——, B. L. Otto-Bliesner, E. C. Brady, C. J. Poulsen, J. E. Tierney, M. Lofverstrom, and P. DiNezio, 2021: Assessment of equilibrium climate sensitivity of the Community Earth System Model version 2 through simulation of the Last Glacial Maximum. *Geophys. Res. Lett.*, **48**, e2020GL091220, https://doi.org/10.1029/2020GL091220.